Shear shock evolution in soft solids

by

Chockalingam Senthilnathan

Submitted to the Department of Aeronautics and Astronautics
in partial fulfillment of the requirements for the degree of

Master of Science in Aeronautics and Astronautics

at the

MASSACHUSETTS INSTITUTE OF TECHNOLOGY

September 2019

© Massachusetts Institute of Technology 2019. All rights reserved.

Signature redacted

Author ....
Department of Aeronautics and Astronautics
August 6, 2019

Signature redacted

Certified by..
Tal Cohen
Assistant Professor of Civil and Environmental Engineering
Assistant Professor of Mechanical Engineering
Thesis Supervisor

Signature redacted

Accepted by ....
Sertac Karaman
Associate Professor of Aeronautics and Astronautics
Chair, Graduate Program Committee

MASSACHUSETTS INSTITUTE OF TECHNOLOGY
OCT 09 2019
LIBRARIES
ARCHIVES

Shear shock evolution in soft solids

by

Chockalingam Senthilnathan

Submitted to the Department of Aeronautics and Astronautics
on August 6, 2019, in partial fulfillment of the
requirements for the degree of
Master of Science in Aeronautics and Astronautics

Abstract

Nonlinear evolution of shear waves into shocks in incompressible elastic materials is investigated using the framework of large deformation elastodynamics, for a family of loadings and commonly used hyperelastic material models. Closed form expressions for the shock formation distance are derived and used to construct non-dimensional phase maps that determine regimes in which a shock can be realized. These maps reveal the sensitivity of shock evolution to the amplitude, shape, and ramp time of the loading, and to the elastic material parameters. In light of a recent study (Espindola et al., 2017), which hypothesizes that shear shock formation could play a significant role in Traumatic Brain Injury (TBI), application to brain tissue is considered and it is shown that the size matters in TBI research. Namely, for realistic loadings, smaller brains are less susceptible to formation of shear shocks. Furthermore, given the observed sensitivity to the imparted waveform and the constitutive properties, it is suggested that the non-dimensional maps can guide the design of protective structures by determining the combination of loading parameters, material dimensions, and elastic properties that can avoid shock formation.

Thesis Supervisor: Tal Cohen
Title: Assistant Professor of Civil and Environmental Engineering
Assistant Professor of Mechanical Engineering

Acknowledgments

I am indebted to my research advisor, Tal Cohen, for allowing me to conduct research under her tutelage and for her guidance and support through this thesis work. I would also like to thank my academic advisor Raul Radovitzky whose experience has been very helpful in navigating my academic program. I am further grateful to the past and present members of Cohen's mechanics group, who were a great source of support throughout this endeavor. I acknowledge with a deep sense of gratitude, the unwavering love and support of my family - Senthilnathan, Vanathy, Seetha, Karpagavalli, Abhinaya, Tiger, and Scooby. Finally, I would like to record my earnest thanks to my friends Ximo Gallud, Zhiyi Wang, and Sooraj Narayan, for making life at MIT easier.

Contents

1 Introduction **11**

2 Nonlinear Shear Wave Equation and Method of Characteristics **15**

2.1 Problem setting 15
2.2 Equation of Motion 18
2.3 Shear shock condition 20
2.4 Method of Characteristics 21

3 Solution to Boundary Value Problem **25**

3.1 General solution to BVP 25
3.2 Shock formation 26
3.3 Acceleration magnification 30
3.4 Immediate shock formation 33
3.5 Solution for a general family of loadings 34

4 Analysis for different nonlinear shear constitutive responses **39**

4.1 Exponential stress model 39
4.2 Gent model 49
4.3 Ogden model 57

5 Example application to shear shock formation in brain tissue **67**

6 Concluding Remarks & Future Work **71**

6.1 Conclusions 71

6.2 Future Work 72

A Solution for loading (3.28) **73**

A.1 Derivation of X_M, t_M^0 73

A.2 Derivation of $\frac{\mathrm{d}t_M^\alpha}{\mathrm{d}\alpha}$ 74

A.3 Application to material models 74

A.3.1 Exponential model 74

A.3.2 Gent model 77

A.3.3 Ogden model 78

B Post first shock formation **81**

List of Figures

2-1 Problem setting - Undeformed and deformed configurations. 16

2-2 Evolution of a loading waveform for a stiffening versus softening material - steepening of waveform into a shock versus spreading of waveform. 21

3-1 Analysis of nonlinear wave evolution and shock formation using characteristics on the $t - X_2$ plane. 24

3-2 Family of loading waveforms being studied. 32

4-1 Dimensionless shear stress and shear wavespeed for the exponential stress model. 35

4-2 a) Representative non-dimensional phase map of the shock location. b) Non-dimensional maps of the shock location for the exponential stress model. 38

4-3 Non-dimensional maps of the location of earliest realization of given acceleration magnification for the exponential stress model (i). 41

4-4 Non-dimensional maps of the location of earliest realization of given acceleration magnification for the exponential stress model (ii). 41

4-5 Dimensionless shear stress and shear wavespeed for the Gent model. . 42

4-6 Dimensionless shear wavespeed for the Gent model as a function of the fractional shear strain. 43

4-7 Quantities related to the minimization of time taken for characteristics to meet, for the Gent model. 45

4-8 Non-dimensional maps of the shock location for the Gent model. . . . 45

4-9 Non-dimensional maps of the location of earliest realization of given acceleration magnification for the Gent model (i). 47

4-10 Non-dimensional maps of the location of earliest realization of given acceleration magnification for the Gent model (ii). 47

4-11 Dimensionless shear stress and shear wavespeed for the two parameter Ogden model. 48

4-12 Two parameter Ogden model: a) Candidate for modified shear strain that minimizes time taken for characteristics to meet. b) Non-dimensional maps of the shock location. 50

4-13 Non-dimensional maps of the location of earliest realization of given acceleration magnification for the two parameter Ogden model (i). . . 52

4-14 Non-dimensional maps of the location of earliest realization of given acceleration magnification for the two parameter Ogden model (ii). . 53

5-1 Shock formation distance in the brain as a function of the ramp velocity for linear loading. 55

Chapter 1

Introduction

Solids are capable of transmitting mechanical shear waves, which can evolve into shocks depending on the nonlinearity of the shear response. Generating such shear shocks in stiff materials, such as metals, would require extreme strain rates at high stress and would lead to catastrophic damage and failure by other competing processes before shock wave phenomena can be observed (Marchand and Duffy, 1988; Mercier and Molinari, 1998). By contrast, even weak impacts can generate shear shocks within small distances in soft solids, owing to their low shear moduli and significantly higher nonlinearity in shear (Catheline et al., 2003). Many soft solids including biological tissues typically have a shear modulus that is orders of magnitude smaller than the bulk modulus and can hence be assumed to be incompressible. This thesis concerns the nonlinear evolution of shear waves into shear shocks in such materials.

Nonlinear shear waves have been studied extensively by both the continuum mechanics and nonlinear acoustics communities. Propagation of finite amplitude plane shear waves and shear shocks were investigated by Chu (1964, 1967), in incompressible isotropic elastic materials. Therein, the condition for shear shock formation was established and the shear loading problem of an incompressible elastic half space was studied using the method of characteristics. Collins (1966, 1967) extended the investigation of wave propagation to materials with transverse isotropy and allowed for transverse displacements in two directions. Davison (1966) studied nonlinear shear waves and propagation of shock waves that are generated by impact loadings in compressible hyperelastic materials wherein accounting for coupled longitudinal motion is necessitated by the compressibility. There, an instantaneous constant loading is considered whereby a shock would immediately form at the loading surface, as opposed to evolution of a smooth loading waveform into shocks as considered by Chu (1964). Recently, Ziv and Shmuel (2019) applied the formulation developed by Davison (1966) to specific compressible hyperelastic material models. Aboudi and Benveniste (1973, 1974) developed a finite-difference based scheme to study such impact induced nonlinear waves. Solutions to the wave equations for compressible hyperelastic materials was provided by Destrade and Saccomandi (2005), including the possibility of dissipation, extending the pioneering works of Carroll (1967, 1974, 1977a,b, 1979).

The nonlinear evolution of shear waves has also been extensively studied in acoustics, where it is routine to perform expansions of the strain energy density function, which is essentially an assumption of weak nonlinearity. The paraxial approximation of small but finite[1] wave amplitudes is also employed to obtain reduced wave equations. A nonlinear parabolic wave equation for shear wave beams in isotropic solids was first derived by Zabolotskaya (1986) accounting for nonlinearity, viscous dissipation and diffraction. In the absence of diffraction, the equation reduces to the Modified Burgers equation (MBE) which is similar to the Burgers equation except the quadratic nonlinearity term is replaced by a cubic one. The MBE was studied in detail by Lee-Bapty and Crighton (1987). An alternative expansion of the strain energy density, suitable for application to soft solids, was provided by Hamilton et al. (2004) and used to derive equations that describe nonlinear propagation of plane shear waves for different polarizations (Zabolotskaya et al., 2004). The plane wave model was extended to account for diffraction by Wochner et al. (2008). Recently, Destrade et al. (2019) extended the formulation to any isotropic incompressible solid without having to rely on expansions of the strain energy density.

While the theoretical investigation of shear shocks in solids dates back to the 60's, the first observation of shear shocks in an elastic medium was only reported recently (Catheline et al., 2003). This was achieved by application of a transient elastography technique to measure the displacements induced by transverse vibrations applied on one end of a gelatin phantom sample. A more recent study by Espíndola et al. (2017) employed a similar method and demonstrated the spontaneous evolution of smooth shear waves into shear shocks in a porcine brain and reported acceleration magnifications of up to a factor of 8.5. Hence, it was suggested that shear shock waves could be an unappreciated damage mechanism that could play a significant role in traumatic brain injury. To reliably study shear shock generation in the brain and other soft solids, it is vital to consider realistic loadings and the possibility of large deformations. However, both the experimental studies discussed, apply harmonic loading, and make use of reduced wave equations and strain energy density expansions that apply for small amplitude deformations and weak nonlinearity.

---

[1] The shear response would be linear for infinitesimal displacements.

In light of these recent studies, in this work we utilize a large deformation elastodynamics framework to study shear shock evolution using realistic constitutive relations that can capture the strongly nonlinear response of soft and biological materials, with the goal of answering the fundamental question: *Can shear shocks be induced in soft materials, such as brain tissue, within the length of the impacted object, when subjected to realistic loadings at large deformations?* To answer the question, we conduct a parametric analysis using three different constitutive relations that capture a wide range of incompressible material response, and a family of loading waveforms.

The thesis is organized as follows: In the following Chapter, we begin by defining our problem setting, deriving the governing equations and introducing the method of characteristics. Then, in Chapter 3, we solve the boundary value problem by employing the method of characteristics, as in Chu (1964), and derive general expressions needed to evaluate the shock formation distance for a family of loadings. Subsequently, in Chapter 4, we apply these expressions to analyze various stress responses, and arrive at closed form expressions for the shock formation distance. These expressions are used to construct non-dimensional phase maps that determine regimes in which a shock can exist and illuminate the effect of material properties and loading scenarios on shock evolution. A parallel supplementary investigation of the distance taken for realization of a given finite acceleration magnification is also carried out.

Finally, in Chapter 5, we demonstrate application of our results to the problem of shear impact of the brain to answer the question posed earlier. We provide some concluding remarks and future research directions in Chapter 6.

Chapter 2

Nonlinear Shear Wave Equation and Method of Characteristics

In this chapter, we begin by defining our problem setting in Sec. 2.1 and then deriving the governing equations in Sec. 2.2. For the resulting nonlinear shear wave equation, we discuss the conditions under which a shock can spontaneously evolve in Sec. 2.3, and then introduce the method of characteristics in Sec. 2.4 to be able to solve the same.

2.1 Problem setting

Consider a homogeneous and isotropic semi-infinite medium whose undeformed stress-free configuration is described by the Lagrangian coordinates $\mathbf{X} = (X_1, X_2, X_3)$, with $-\infty < X_1, X_3 < \infty$, and $X_2 \geq 0$, as shown in Fig. 2-1(a). The body is subjected to shearing motion by imposition of a continuous time dependent shearing velocity $V(t)$, on its surface $X_2 = 0$, along X_1 as shown in Fig. 2-1(b). Using symmetry considerations and incompressibility, the mapping between the Lagrangian coordinates of a material point, $\mathbf{X}$, and its current coordinates, $\mathbf{x}$, at time t, is necessarily given by

$$x_1 = X_1 + u(X_2, t), \qquad x_2 = X_2, \qquad x_3 = X_3 \tag{2.1}$$

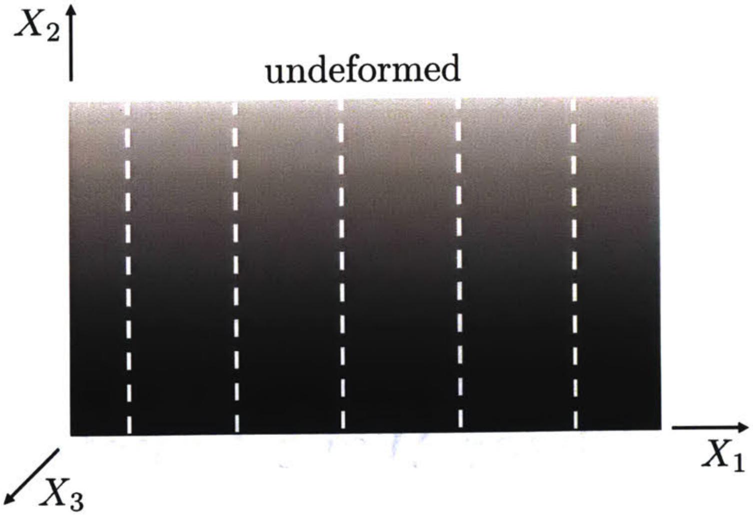

(a) The initial undeformed configuration.

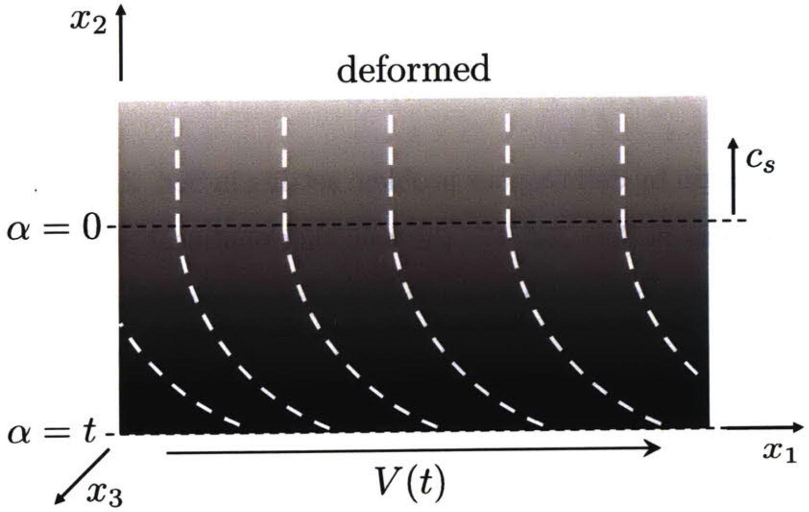

(b) Deformed configuration where a continuous time varying shearing velocity $V(t)$ is applied on the surface $X_2 = 0$. The wavefront, $\alpha = 0$ (see Chapter 3), travels at the linear elastic shear wavespeed c_s (before shock formation).

Figure 2-1: Dynamic simple shear deformation of a homogeneous isotropic perfectly incompressible material occupying the half-space $X_2 \geq 0$. The white dashed lines are shown to observe the shear deformation.

where $u(0, t) = \int_0^t V(t)\mathrm{d}t$ is the shear displacement of the surface $X_2 = 0$. The shear strain $\gamma(X_2, t)$ is given by

$$\gamma(X_2, t) = \frac{\partial x_1}{\partial X_2} = \frac{\partial u(X_2, t)}{\partial X_2} \tag{2.2}$$

and the particle velocity is given by

$$v(X_2, t) = \frac{\partial u(X_2, t)}{\partial t} \quad \text{where} \quad v(0, t) = V(t) \tag{2.3}$$

The deformation gradient $\mathbf{F}$ and the left Cauchy Green deformation tensor $\mathbf{B}$ can then be written as

$$\mathbf{F} = \frac{\partial \mathbf{x}}{\partial \mathbf{X}} = \begin{bmatrix} 1 & \gamma & 0 \\ 0 & 1 & 0 \\ 0 & 0 & 1 \end{bmatrix} \quad , \quad \mathbf{B} = \mathbf{F} \cdot \mathbf{F}^T = \begin{bmatrix} \gamma^2 + 1 & \gamma & 0 \\ \gamma & 1 & 0 \\ 0 & 0 & 1 \end{bmatrix} \tag{2.4}$$

and the invariants of $\mathbf{B}$ are given by $I_1 = I_2 = 3 + \gamma^2$ and $J = \det(\mathbf{F}) = 1$.

In our analysis we consider a purely mechanical theory and restrict our attention to incompressible hyperelastic materials. The strain energy density per unit volume, W, can then be written in its most general form as

$$W = W(I_1, I_2) \tag{2.5}$$

Defining $W_i = \frac{\partial W}{\partial I_i}$ for $i = 1, 2$, the first Piola-Kirchhoff stress tensor $\mathbf{P}$ and the Cauchy stress $\mathbf{T}$ are given by

$$\mathbf{P} = \mathbf{T}\mathbf{F}^{-T} \quad , \quad \mathbf{T} = -p\,\mathbf{1} + 2\big[(W_1 + I_1 W_2)\mathbf{B} - W_2 \mathbf{B}^2\big] \tag{2.6}$$

where $p = p(X_2, t)$ is a pressure field that arises due to the incompressibility constraint and is determined by the boundary value problem. Substituting the deformation field (2.4) in (2.6), we arrive at a stress state of the form[1]

$$\mathbf{P}(X_2, t) = \begin{bmatrix} 2W_1 + 4W_2 - p & 2\gamma(W_1 + W_2) & 0 \\ \gamma(-2W_2 + p) & 2W_1 + 4W_2 - p & 0 \\ 0 & 0 & 2W_1 + 4W_2 + 2\gamma^2 W_2 - p \end{bmatrix} \tag{2.7}$$

---

[1] Note that different authors (ex: Chu (1964), Horgan and Murphy (2011)) might report seemingly different longitudinal stress expressions for the simple shear problem, but they all differ only by a hydrostatic term which can be absorbed into the undetermined pressure field p.

where the stress component $P_{12}(=T_{12})$ is denoted by $\tau(\gamma)(=2\gamma(W_1+W_2))$ and is referred to as the shear stress. Note that $\tau(\gamma)$ is an odd function.

2.2 Equation of Motion

While dilatational stresses are transmitted instantaneously in an incompressible elastic medium, shear stresses are transmitted at a finite velocity. As the surface $X_2=0$ is put to motion to generate deformation, a shear wave propagates into the undeformed material and its propagation is governed by balance of linear momentum, which, in absence of body forces, reads

$$\int_{\mathcal{D}_0} \rho_0 \dot{\mathbf{v}} \mathrm{dV}_0 = \int_{\partial\mathcal{D}_0} \mathbf{P}\mathbf{n}_0 \mathrm{dA}_0 \tag{2.8}$$

Here $\dot{\mathbf{v}}$ is the material acceleration, ρ_0 is the constant density, and integration is performed on a subregion $\mathcal{D}_0$ in the reference configuration. In the absence of shocks, assuming the smoothness of fields, this balance law can be localized as

$$\mathrm{Div}\ \mathbf{P} = \rho_0 \dot{\mathbf{v}} \tag{2.9}$$

Substituting (2.7) into (2.9) gives us the following equations,

$$\frac{\partial \tau}{\partial X_2} = \rho_0 \frac{\partial^2 u}{\partial t^2} \tag{2.10a}$$

$$\frac{\partial P_{22}}{\partial X_2} = 0 \Rightarrow \frac{\partial p}{\partial X_2} = \frac{\partial(2W_1+4W_2)}{\partial X_2} \tag{2.10b}$$

While perfect incompressibility allows us to impose an arbitrary normal traction $\sigma_n = P_{22}$ that will be instantaneously equilibrated throughout the body (as seen from (2.10b)), in a compressible material, coupling between the longitudinal and shearing deformations might become significant (see for example Ziv and Shmuel (2019)).

Plugging (2.2) into (2.10a) gives us the nonlinear wave equation

$$\frac{\partial^2 u}{\partial t^2} = c^2 \frac{\partial^2 u}{\partial X_2^2} \quad \text{where} \quad c(\gamma) = \sqrt{\frac{1}{\rho_0}\frac{\partial \tau}{\partial \gamma}} \tag{2.11}$$

where in writing the expression for the wavespeed $c(\gamma)$ the tacit assumption has been made that $\tau'(\gamma) > 0$, to ensure hyperbolicity of the wave equation such that shear stresses are transmitted through waves. Note that $c(\gamma)$ is an even function. At the linear elastic limit shear waves are transmitted at the constant wavespeed c_s given by

$$c_s = \lim_{\gamma \to 0} c(\gamma) = \sqrt{\frac{\mu}{\rho_0}} \tag{2.12}$$

where μ is the linear elastic shear modulus. In terms of strain and velocity, written in (2.2) and (2.3), equation (2.11) can be written as a system of equations,

$$\frac{\partial v}{\partial t} = c^2 \frac{\partial \gamma}{\partial X_2} \tag{2.13a}$$

$$\frac{\partial \gamma}{\partial t} = \frac{\partial v}{\partial X_2} \tag{2.13b}$$

where (2.13b) is the compatibility condition.

It should be noted that, in practice, the simple shear deformation (2.4) is a nontrivial one to generate, especially in the large deformation settings, as it requires suitable tractions to be applied on the inclined surfaces, see Destrade et al. (2012), Horgan and Murphy (2011), and Horgan and Murphy (2012). Generating a dynamic simple shear deformation in finite dimensional blocks would be even more tedious, requiring time and spatially varying tractions on the inclined surfaces and would not correspond to any real life shearing scenarios. In the present study we consider shearing of an elastic half-space which can be considered an approximation of a physical shearing setting with large in-plane dimensions $X_1 - X_3$, such that effects from the free surfaces can be neglected in the mid-section where the deformation can be assumed to be one of simple shear.

2.3 Shear shock condition

The shear wavespeed c in (2.11) is a function of the local shear strain $\gamma(X_2, t)$. Hence, if the local wavespeed increases along the wave propagation direction, a given wave form will spatially spread over time. On the other hand, if the wavespeed decreases along the propagation direction, the waveform would steepen spatially over time and can eventually develop a local discontinuity when a shock forms. Accordingly, for a shear wave travelling in the positive X_2 direction, shocks can form when $\frac{\partial c}{\partial X_2} = \frac{\mathrm{d}c}{\mathrm{d}\gamma}\frac{\partial \gamma}{\partial X_2} < 0$. Hence, using the expression for $c(\gamma)$ from (2.11) and the fact that $\tau(\gamma)$ is an odd function, we obtain the condition for shear shock formation as[2]

$$\tau''(|\gamma|)\frac{\partial|\gamma|}{\partial X_2} < 0 \tag{2.14}$$

Formation of a shock thus depends on the loading program - loading or unloading the material, as defined by the sign of $\frac{\partial|\gamma|}{\partial X_2}$ and on the nonlinear shear response of the material through the sign of $\tau''(|\gamma|)$. A material with shear stress response such that $\tau''(|\gamma|) > 0$ will thus evolve a smooth shear loading waveform into a shock when it is being sheared, and one with a shear stress response such that $\tau''(|\gamma|) < 0$ will produce a shear shock when unloaded from a sheared state. Fig. 2-2 shows a loading shear waveform steepening into a shear shock versus spreading out, depending on the material constitutive shear response. If $\tau''(\gamma) = 0$, that is if the material shear response is linear ($\tau = \mu\gamma$) and the wavespeed is constant, the waveform will be relayed at the constant speed c_s without steepening or spreading out (dashed lines in Fig. 2-2).

The most commonly used neo-Hookean (Rivlin, 1948) and Mooney-Rivlin (Mooney, 1940) hyperelastic models both predict a linear shear stress response, in which case there would be no nonlinear shear wave evolution. Biological tissues such as the brain have a strain stiffening shear response (Mihai et al., 2017, 2015; Pogoda et al.,

---

[2] Here we have used the definitions $\tau''(|x|) \equiv \tau''(\gamma)\big|_{\gamma=|x|}$, $\frac{\partial|\gamma|}{\partial X_2} \equiv \frac{\partial(\gamma \mathrm{sign}(\gamma))}{\partial X_2}$, and we consider situations in which shear strain does not change sign. Also, whenever we discuss sign of $\tau''(|\gamma|)$ we consider non-zero shear strains.

2014; Storm et al., 2005) and unsurprisingly commonly used hyperelastic models for soft solids and biological tissues such as the Gent model (Gent, 1996; Horgan, 2015) and the Fung model (Fung, 1993) predict stiffening shear response i.e $\tau''(|\gamma|) > 0$ (see Mihai et al. (2015)). Thus soft tissues and other materials whose constitutive response is well captured by these models would allow for shock formation in shear loading. Hence, in this work, we focus our attention on shear loading (as opposed to unloading from a pre-sheared state). Note that the velocity V and the strain γ will be of opposite signs by virtue of their definition. Thus when the elastic half-space is sheared along positive X_1 direction (i.e $V > 0$) it develops a negative shear strain.

While (2.14) gives us the condition under which a shear wave can nonlinearly evolve into a shock, it does not provide information about the length and time scales over which the nonlinear evolution of the smooth waveform into a shock happens, or how this evolution depends on the material nonlinearity and the waveform. To that end, we will analyze the transient evolution of shear waves up to shock formation. We will then apply the analysis to different constitutive stress responses.

2.4 Method of Characteristics

To investigate the transient evolution of shear waves we follow the formulation in Chu (1964) (results recapitulated here) which makes use of the method of characteristics, we first introduce the auxiliary function $Q(\gamma)$ and its derivatives

$$Q(\gamma) = \int_0^\gamma c(\gamma)\mathrm{d}\gamma, \qquad \frac{\partial Q}{\partial t} = c(\gamma)\frac{\partial \gamma}{\partial t}, \qquad \frac{\partial Q}{\partial X_2} = c(\gamma)\frac{\partial \gamma}{\partial X_2} \tag{2.15}$$

The monotonicity of Q ensures that a unique value corresponds to a given shear strain γ. Further, $Q(\gamma)$ is an odd function ($Q(-\gamma) = -Q(\gamma)$) as $c(\gamma)$ is an even function. Using the above definitions, we can reduce the system of equations (2.13) to the two

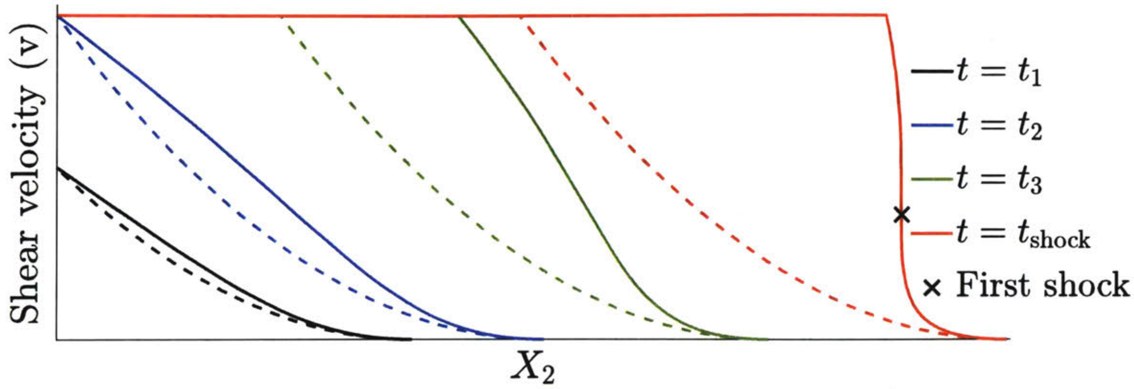

(a) Material with stiffening shear stress response, i.e $\tau''(|\gamma|) > 0$. Here, $t_1 < t_2 < t_3 < t_{\text{shock}}$. The figure was made for the exponential stress model (4.1), and the parameters chosen were such that the loading was in the regime $m > m_{\text{th}}$ (and $n > n_c = 1$) so that the first shock forms somewhere in the middle of the ramping part of the waveform (see Sec. 4.1).

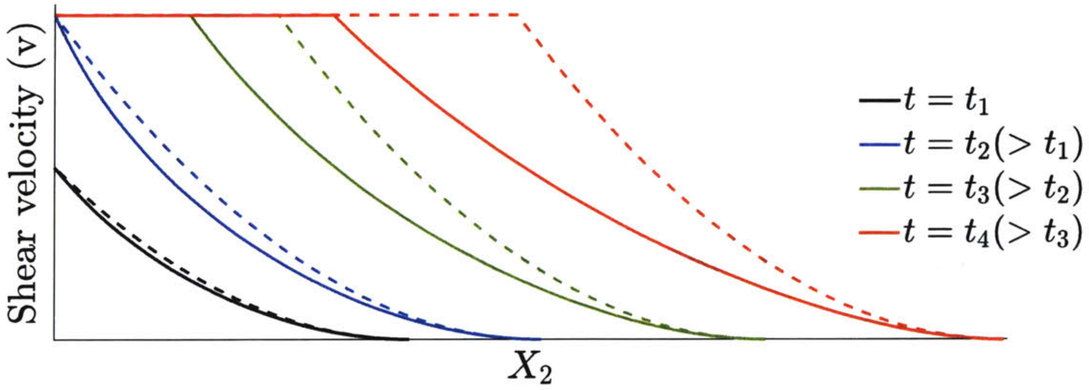

(b) Material with softening shear response i.e $\tau''(|\gamma|) < 0$. Figure is a representative one for a general softening solid.

Figure 2-2: A quadratic loading waveform ($n = 2$ in (3.28)) nonlinearly evolving while being spatially relayed by a material. The dashed lines represent the response of a material with a linear shear stress response.

ordinary differential equations,

$$\begin{aligned} \frac{\partial(v+Q)}{\partial t} - c(\gamma)\frac{\partial(v+Q)}{\partial X_2} &= 0 \\ \frac{\partial(v-Q)}{\partial t} + c(\gamma)\frac{\partial(v-Q)}{\partial X_2} &= 0 \end{aligned} \tag{2.16}$$

whose solution can be shown to be

$$v + Q = f(\beta) \quad \text{and } v - Q = g(\alpha) \tag{2.17a}$$

$$\text{where} \quad \mathrm{d}\beta = 0 \ \text{ along } \ \frac{\mathrm{d}X_2}{\mathrm{d}t} = -c \quad \text{and } \mathrm{d}\alpha = 0 \ \text{ along } \ \frac{\mathrm{d}X_2}{\mathrm{d}t} = c \tag{2.17b}$$

The variables α and β identify sets of characteristic curves described by $\frac{\mathrm{d}X_2}{\mathrm{d}t} = \pm c$ along which characteristic relations $\mathrm{d}v = \pm c\,\mathrm{d}\gamma$ hold. The general solution (2.17) can be applied to our boundary value problem to solve for the transient shear wave evolution up to formation of shocks. Upon formation of discontinuities the assumption of smoothness used to localize the integral form of momentum balance (2.8) breaks down, and thus the method of characteristics solution will not hold in regions with shocks.

Chapter 3

Solution to Boundary Value Problem

This chapter is organized as follows: In Sec. 3.1, we formally pose the boundary value problem (BVP) for the problem setting described in the previous chapter and provide the solution for a general loading using the method of characteristics discussed in Sec. 2.4. The distance from the loading surface at which shock formation initiates is discussed in Sec. 3.2 and the distance for earliest realization of a given acceleration magnification is discussed in Sec. 3.3. The condition under which shock formation can initiate immediately at the loading surface is examined in Sec. 3.4. Finally, in Sec. 3.5, the general solution to the BVP is specialized for a family of loading waveforms and general expressions are derived which are used to analyze different constitutive models in the next chapter.

3.1 General solution to BVP

Summarising our boundary value problem we have the initial and boundary conditions

$$v(X_2 \geq 0, t = 0) = 0 \quad , \quad \gamma(X_2 \geq 0, t = 0) = 0 \quad , \quad v(X_2 = 0, t > 0) = V(t) \quad (3.1)$$

where we consider $V(t)$ to be a continuous piece-wise differentiable function of t. Using the method of characteristics, the solution for the velocity and strain fields is[1]

---

[1] There is no dependence on β (from (2.17)) as the initial shear strain in the body is constant (and zero).

(Chu, 1964),

$$\hat{v}(\alpha) = V(\alpha) \tag{3.2a}$$

$$\hat{Q}(\alpha) = -V(\alpha) \quad \xrightarrow{(2.15)^1} \quad V(\alpha) = -\int_0^{\hat{\gamma}(\alpha)} c(\gamma)\mathrm{d}\gamma \tag{3.2b}$$

where fields written as a function of α have $\hat{()}$ accents and, as such, $\hat{Q}(\alpha) = Q(\hat{\gamma}(\alpha))$. According to (3.2), the velocity v and shear strain γ (or equivalently Q) are constant along characteristic lines identified by the characteristic variable α. The equation of a characteristic line identified by α is (Chu, 1964)

$$X_2 = \hat{c}(\alpha)(t - \alpha) \tag{3.3}$$

where $\hat{c}(\alpha) = c(\hat{\gamma}(\alpha))$ and the characteristics are labelled such that $\alpha = t$ on $X_2 = 0$ so that the characteristic α sets out from the loading surface at $t = \alpha$. Equation (3.3) determines a relation

$$\alpha = \alpha(X_2, t) \tag{3.4}$$

which allows us to convert the solution field from functions of α to functions of (X_2, t). When characteristics meet, a shock is formed, α becomes multivalued at a given (X_2, t), and the solution (3.2) is invalid beyond this time as previously discussed in Sec. 2.4. In this work we are only concerned with the transient nonlinear evolution of shear waves up to the first formation of a shock.

3.2 Shock formation

We now apply the formulas from the previous section to evaluate the length and time scales needed for the development of a shock discontinuity. Representative characteristic lines in the $t - X_2$ plane are shown in Fig. 3-1(a). The slope of a characteristic line setting out at the loading surface $X_2 = 0$ at time $t = \alpha$ is $1/\hat{c}(\alpha)$. Consider two characteristics described by some $\alpha > 0$ and $\alpha + \mathrm{d}\alpha > 0$, that set out from the load-

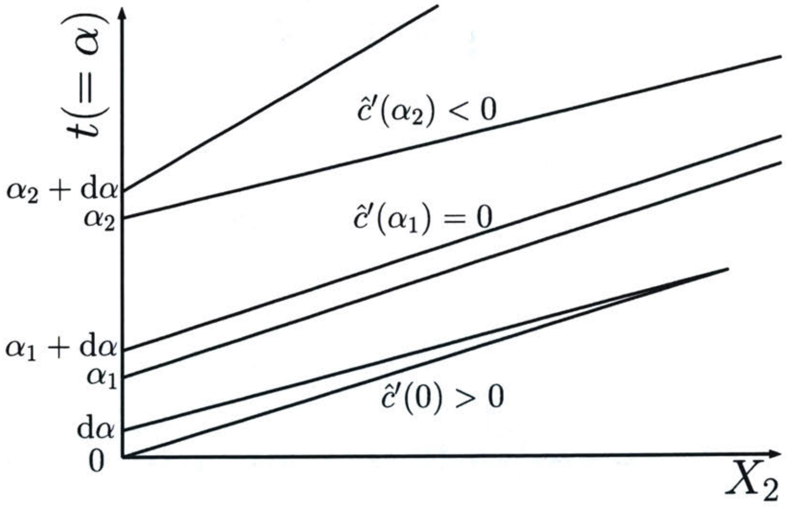
$t(=\alpha)$
$\alpha_2 + \mathrm{d}\alpha$
α_2
$\alpha_1 + \mathrm{d}\alpha$
α_1
$\mathrm{d}\alpha$
0
$\hat{c}'(\alpha_2) < 0$
$\hat{c}'(\alpha_1) = 0$
$\hat{c}'(0) > 0$
X_2

(a) Characteristics with slope $1/c$ on the $t - X_2$ plane, described by (3.3), along which shear velocity and strain are constant. In regions where the characteristics run away from each other ($\hat{c}' < 0$) the waveform spatially spreads with time and in regions where their separation reduces ($\hat{c}' > 0$) the waveform steepens. In regions where characteristics are parallel ($\hat{c}' = 0$) the waveform is locally relayed with no nonlinear evolution. When characteristics run into each other, shear shocks are formed, causing discontinuous strain and velocity fields.

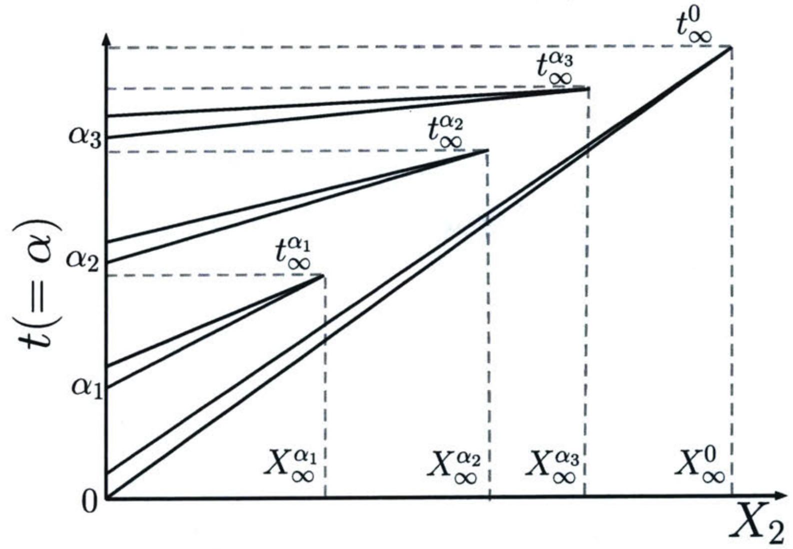
t^0_∞
$t^{\alpha_3}_\infty$
$t^{\alpha_2}_\infty$
$t^{\alpha_1}_\infty$
α_3
α_2
α_1
$t(=\alpha)$
0
$X^{\alpha_1}_\infty$
$X^{\alpha_2}_\infty$
$X^{\alpha_3}_\infty$
X^0_∞
X_2

(b) The earliest time at which characteristics run into each other is the time at which the first shear shock is formed, i.e $t^{\text{shock}} = t^{\alpha_1}_\infty$ for the figure shown. At later times ($t > t^{\text{shock}}$) the solution using method of characteristics breaks down and jump conditions would have to be applied at the location of the shock. The location at which the characteristics meet earliest can also be shown to be the shortest distance from the loading surface at which characteristics meet.

Figure 3-1: Analysis using characteristics on the $t - X_2$ plane.

ing surface within an infinitesimal time separation $\mathrm{d}\alpha$, with slopes $1/\hat{c}$ and $1/(\hat{c}+\mathrm{d}\hat{c})$ respectively; if $\hat{c}' > 0$ they can meet and form a shock at a time

$$t_\infty^\alpha = \alpha + \frac{\hat{c}}{\hat{c}'}\,, \qquad t_\infty^\alpha > \alpha \tag{3.5}$$

and at the location (using (3.3))

$$X_\infty^\alpha = \hat{c}(t_\infty^\alpha - \alpha) = \frac{\hat{c}^2}{\hat{c}'} \tag{3.6}$$

where, from here on, quantities with the superscript α are assosciated with the characteristic line α. Since $c(\gamma)$ is an even function, we have $c(\gamma) = c(|\gamma|)$. Thus we have $\hat{c}' = \frac{\partial c}{\partial|\gamma|}\frac{\mathrm{d}|\hat{\gamma}|}{\mathrm{d}\alpha}$ where the sign of $\frac{\mathrm{d}|\hat{\gamma}|}{\mathrm{d}\alpha} = \frac{\mathrm{d}|\gamma(0,t)|}{\mathrm{d}t}$ is decided by the loading program (positive for loading and negative for unloading) and $\frac{\partial c}{\partial|\gamma|}$ has the same sign as $\tau''(|\gamma|)$. Thus, the shock condition $\hat{c}' > 0$ implies that a strain stiffening material ($\tau''(|\gamma|) > 0$) would develop shocks under shear loading and a strain softening material ($\tau''(|\gamma|) < 0$) would develop shear shocks in unloading. This is consistent with the discussion in Sec. 2.3.

From (3.5) and (3.6), the time and distance taken for characteristics to meet depend inversely on $\hat{c}' = \frac{\mathrm{d}c}{\mathrm{d}\gamma}\hat{\gamma}'$, where $\frac{\mathrm{d}c}{\mathrm{d}\gamma}$ is smaller in magnitude for materials with weaker nonlinearity of shear response, and $\frac{\mathrm{d}\hat{\gamma}}{\mathrm{d}\alpha} = \frac{\mathrm{d}\gamma(0,t)}{\mathrm{d}t}$ is the strain rate generated at the loading surface which can be related to the velocity loading rate by differentiating (3.2b),

$$V'(\alpha) = -c\frac{\mathrm{d}\hat{\gamma}}{\mathrm{d}\alpha} \qquad \text{i.e} \qquad \frac{\mathrm{d}V}{\mathrm{d}t} = -c\frac{\mathrm{d}\gamma(0,t)}{\mathrm{d}t} \tag{3.7}$$

Accordingly, (3.5) and (3.6) can be written as

$$t_\infty^\alpha = \alpha + \frac{\hat{\psi}}{V'(\alpha)} \quad \text{where} \quad \hat{\psi} = \psi(\hat{\gamma}) \quad \text{and} \quad \psi(\gamma) = -c^2\left(\frac{\mathrm{d}c}{\mathrm{d}\gamma}\right)^{-1} \tag{3.8a}$$

$$X_\infty^\alpha = \frac{\hat{\psi}\hat{c}}{V'(\alpha)} \tag{3.8b}$$

Functions of α can be rewritten as functions of the strain and vice versa using (3.2b), i.e $\hat{F}(\alpha) = F(\hat{\gamma}(\alpha))$. Thus higher the loading rate ($|V'|$) and/or stronger the material nonlinearity (higher $|\frac{\mathrm{d}c}{\mathrm{d}\gamma}|$), the quicker the characteristics meet and over shorter distances.

The velocity gradient on a given characteristic α, denoted by $v^{\alpha}_{X_2}$, can be found using (3.2a) and (3.3) as function of the time $t(> \alpha)$ or location X_2,

$$v^{\alpha}_{X_2} = \frac{\partial \hat{v}(\alpha(X_2,t))}{\partial X_2} = \hat{v}' \frac{\partial \alpha}{\partial X_2} \ , \ v^{\alpha}_{X_2}(X_2) = \frac{V'(\alpha)}{\hat{c}' X_2/\hat{c} - \hat{c}} \ , \ \tilde{v}^{\alpha}_{X_2}(t) = \frac{V'(\alpha)}{\hat{c}'(t-\alpha) - \hat{c}} \tag{3.9}$$

Similarly, the strain gradient, $\gamma^{\alpha}_{X_2}$, can be found using (3.7) and (3.9), as

$$\gamma^{\alpha}_{X_2} = \frac{\partial \hat{\gamma}(\alpha((X_2,t))}{\partial X_2} = \hat{\gamma}' \frac{\partial \alpha}{\partial X_2} = -\frac{V'(\alpha)}{\hat{c}} \frac{\partial \alpha}{\partial X_2} = -\frac{v^{\alpha}_{X_2}}{\hat{c}} \tag{3.10}$$

Thus, using (3.5) or (3.6) in (3.9) and (3.10), it can be seen that when characteristics meet the magnitude of local spatial gradients of the velocity and strain become infinite. The local acceleration on a given characteristic α, denoted by a^{α}, can be also written as a function of X_2 or t using (3.2a) and (3.3),

$$a^{\alpha} = \frac{\partial \hat{v}(\alpha(X_2,t))}{\partial t} = \hat{v}' \frac{\partial \alpha}{\partial t} \ , \ a^{\alpha}(X_2) = \frac{V'(\alpha)}{1-(\hat{c}'/\hat{c}^2)X_2} \ , \ \tilde{a}^{\alpha}(t) = \frac{V'(\alpha)}{1-(\hat{c}'/\hat{c})(t-\alpha)} \tag{3.11}$$

and its magnitude is also seen to become infinite when characteristics meet (using (3.5) or (3.6) in (3.11)).

The earliest time at which characteristics meet is when the first shock forms and the method of characteristics solution will not hold at later times. Fig. 3-1(b) shows a set of representative charactersitics starting out at different times α_i meeting at different times $t^{\alpha_i}_{\infty}$, the earliest time at which characteristics meet, $t^{\alpha_1}_{\infty}$, is the time at which the first shock forms. Thus, in the general case, the time at which the first shock is formed is given by

$$t^{\text{shock}} = \min_{\alpha \in [0,\infty)} t^{\alpha}_{\infty} \tag{3.12}$$

Using (3.8b), the location at which it forms, denoted by X_{shock}, can be found as

$$X_{\text{shock}} = X^{\alpha}_{\infty}\Big|_{\alpha^{\infty}_{\min}} = \frac{\hat{\psi}\hat{c}}{V'(\alpha)}\Big|_{\alpha^{\infty}_{\min}} \quad \text{where} \quad \alpha^{\infty}_{\min} = \arg\min_{\alpha \in [0,\infty)} t^{\alpha}_{\infty} \tag{3.13}$$

The characteristics that start out at $t = \alpha_{\text{min}}^{\infty}$ are the ones that meet earliest in time to form a shock. When X_{∞}^{α} and t_{∞}^{α} are smooth functions of α, which is true when the material response and loading are smooth (from (3.8)), we can differentiate (3.6) and use (3.5) to write

$$\frac{\mathrm{d}X_{\infty}^{\alpha}}{\mathrm{d}\alpha} = \hat{c}'(t_{\infty}^{\alpha} - \alpha) + \hat{c}\left(\frac{\mathrm{d}t_{\infty}^{\alpha}}{\mathrm{d}\alpha} - 1\right) = \hat{c}\frac{\mathrm{d}t_{\infty}^{\alpha}}{\mathrm{d}\alpha} \tag{3.14}$$

Thus the sign of $\frac{\mathrm{d}X_{\infty}^{\alpha}}{\mathrm{d}\alpha}$ and $\frac{\mathrm{d}t_{\infty}^{\alpha}}{\mathrm{d}\alpha}$ will be the same and $\alpha_{\text{min}}^{\infty}$ will also be a minimizer of X_{∞}^{α}, that is,

$$\alpha_{\text{min}}^{\infty} = \underset{\alpha \in [0,\infty)}{\arg\min}\, X_{\infty}^{\alpha} \tag{3.15}$$

Hence, among the locations of intersection of characteristics, the location at which the first shock forms, X_{shock}, is also at the shortest distance from the loading surface, when the loading and material behaviour are smooth.

3.3 Acceleration magnification

While the spatial steepening of a waveform ultimately results in a shock, we would also like to quantify the nonlinear evolution of the shear wave as it progresses into the material. One way to do this is to analyse the magnification in acceleration along a characteristic with respect to the initial imposed acceleration. Physical systems are finite in length and we might be interested in knowing if a shock can form within a certain length for a given loading and if not what the maximum magnification in acceleration or field gradients would be, since higher velocity and strain gradients or equivalently higher accelerations, can cause damage in the material. Also, real materials are not perfectly elastic, they have some viscosity which has a spatial smoothening influence on the evolving waveform, hence a pure shock (discontinous fields) is never achieved, so it makes sense to talk in terms of acceleration/field gradient magnification which is a staple of nonlinear wave evolution irrespective of whether viscosity is included in the modelling.

The magnification in acceleration along a characteristic α with respect to the imposed acceleration at the loading surface ($a(X_2 = 0, t = \alpha)$), can be written as a function of progressing t or X_2 using (3.11),

$$M^{\alpha}(X_2) = \frac{a^{\alpha}(X_2)}{a^{\alpha}(0)} = \frac{1}{1 - (\hat{c}'/\hat{c}^2)X_2} \quad , \quad \tilde{M}^{\alpha}(t) = \frac{\tilde{a}^{\alpha}(t)}{\tilde{a}^{\alpha}(\alpha)} = \frac{1}{1 - (\hat{c}'/\hat{c})(t - \alpha)} \tag{3.16}$$

Using (3.9), (3.10), and (3.16), it can be shown that the magnification in the velocity and strain gradients along a characteristic α, with respect to their values at the loading surface, is equal to the magnification in acceleration, M^{α},

$$\frac{v^{\alpha}_{X_2}(X_2)}{v^{\alpha}_{X_2}(0)} = \frac{1}{1 - (\hat{c}'/\hat{c}^2)X_2} = M^{\alpha} \quad , \quad \frac{\gamma^{\alpha}_{X_2}(X_2)}{\gamma^{\alpha}_{X_2}(0)} = \frac{v^{\alpha}_{X_2}(X_2)}{v^{\alpha}_{X_2}(0)} = M^{\alpha} \tag{3.17}$$

Thus, henceforth, whenever we talk about magnification in acceleration, it is tantamount to talking about magnification in the velocity or strain gradients.

From (3.16), it can be seen that when $\hat{c}' > 0$ (converging characteristics in the $t - X_2$ plane as shown in Fig. 3-1(a)), the magnitudes of velocity gradient, strain gradient, and acceleration, along a characteristic α, magnify as the wave progresses into the material and become infinite when characteristics meet and form a shock (seen by using (3.5) and (3.6) in (3.16)). On the other hand, when $\hat{c}' < 0$ (diverging characteristics in Fig. 3-1(a)), the magnitudes of acceleration and field gradient along the characteristic decrease, and the wave locally spreads out. If $\hat{c}' = 0$ (parallel characteristics in Fig. 3-1(a)) there is no magnification of fields. For a material with linear shear response $\hat{c}' = \frac{\mathrm{dc}}{\mathrm{d}\gamma}\hat{\gamma}' = 0$ everywhere and the imposed waveform is relayed with no nonlinear evolution at the constant linear elastic shear wavespeed ($v(X_2, t) = V(t - X_2/c_s)$ using (3.2a) and (3.3)). Since we are considering the loading of strain stiffening materials in this thesis, the discussion hereon is for[2] $\hat{c}' \geq 0$.

From (3.16), the time at which a given magnification in acceleration, M, is achieved along a characteristic α, denoted by t^{α}_{M} , is given by

$$t^{\alpha}_{M} = \alpha + \lambda_M \frac{\hat{c}}{\hat{c}'} \qquad \text{where} \qquad \lambda_M = 1 - \frac{1}{M} \tag{3.18}$$

---

[2] Recall that $\hat{c}' = \frac{\mathrm{dc}}{\mathrm{d}\gamma}\hat{\gamma}'$. At zero shear strain, $\frac{\mathrm{dc}}{\mathrm{d}\gamma}$ can be zero, and thus $\hat{c}'$ can be zero.

and the location at which it is achieved is given using (3.3) and (3.18) as

$$X_M^\alpha = \hat{c}(t_M^\alpha - \alpha) = \lambda_M \frac{\hat{c}^2}{\hat{c}'} \tag{3.19}$$

Note that for $\hat{c}' \geq 0$ and $t < t_\infty^\alpha$, $M \in [1, \infty)$ using (3.16) and thus $\lambda_M \in [0, 1)$. The earliest time at which an acceleration magnification M is realized in the material, t_M, and the characteristic along which it is realized earliest, α_{min}^M , are given by

$$t_M = \min_{\alpha \in [0,\infty)} t_M^\alpha \quad , \quad \alpha_{\text{min}}^M = \arg\min_{\alpha \in [0,\infty)} t_M^\alpha \tag{3.20}$$

and the location at which the acceleration magnification M is realized earliest, X_M , is given by (using (3.19) and (3.20))

$$X_M = X_M^\alpha \Big|_{\alpha_{\text{min}}^M} = \lambda_M \frac{\hat{c}^2}{\hat{c}'} \Big|_{\alpha_{\text{min}}^M} \tag{3.21}$$

Using (3.7) we can rewrite eqs. (3.18)–(3.21) as

$$t_M^\alpha = \alpha + \lambda_M \frac{\hat{\psi}}{V'(\alpha)} \quad , \quad t_M = \min_{\alpha \in [0,\infty)} t_M^\alpha \tag{3.22a}$$

$$X_M = \lambda_M \frac{\hat{\psi}\hat{c}}{V'(\alpha)} \Bigg|_{\alpha_{\text{min}}^M} \tag{3.22b}$$

When the loading and material behaviour are smooth, we can differentiate (3.19) and use (3.18) to write

$$\frac{\mathrm{d}X_M^\alpha}{\mathrm{d}\alpha} = \hat{c}'(t_M^\alpha - \alpha) + \hat{c}\left(\frac{\mathrm{d}t_M^\alpha}{\mathrm{d}\alpha} - 1\right) = \hat{c}\left(\frac{\mathrm{d}t_M^\alpha}{\mathrm{d}\alpha} + (\lambda_M - 1)\right) \tag{3.23}$$

Note that for a finite magnification M, we have $\lambda_M < 1$ and thus, the signs of $\frac{\mathrm{d}X_M^\alpha}{\mathrm{d}\alpha}$ and $\frac{\mathrm{d}t_M^\alpha}{\mathrm{d}\alpha}$ need not be the same. Hence, in general, α_{min}^M need not be the minimizer of X_M^α and thus, the location at which a given finite acceleration magnification is realized earliest in time need not be the shortest distance from the loading surface at which it is realized. The analysis for shock formation from the previous section is related to the acceleration magnification analysis by taking the limit $M \to \infty$, namely,

$$\{t_{\infty}^{\alpha},\ t^{\text{shock}},\ \alpha_{\min}^{\infty},\ X_{\text{shock}}\} = \lim_{M\to\infty}\{t_{M}^{\alpha},\ t_{M},\ \alpha_{\min}^{M},\ X_{M}\} \tag{3.24}$$

From eqs. (3.9)–(3.11) and eqs. (3.16)–(3.17), it can be seen that a local discontinuity in the imposed waveform ($V' \to \infty$) would mean infinite local acceleration and field gradients but not necessarily an infinite magnification. By basing our investigation on analysis of the acceleration magnification (3.16), we distinguish between two types of discontinuities: those that are evolved due to nonlinearity of the material; and those that are imposed by a discontinuity in the loading waveform $V(t)$. The discussion of shock waves in this thesis refers to the former, which is associated with the intersection of characteristics, and in turn represents the limit of acceleration/field gradient magnification becoming infinite. The question may arise as to why one might want to draw the distinction between an imposed and a nonlinearly evolved discontinuity; in a physical system with even minute viscosity a high imposed local gradient would be immediately smoothened and a linear material will not try to steepen the smooth wave into a shock, whereas in a nonlinear material (with $\tilde{c}' < 0$), the material would continuously try to steepen the waveform, increasing the strength of the field gradients/acceleration with time while the viscosity tries to dissipate them away (Bland, 1965).

3.4 Immediate shock formation

If the very first characteristics ($\alpha \to 0^+$) meet immediately, then a shock is instantaneously formed at $(t, X_2) = (0, 0)$ and there would be no need to perform the minimisation in (3.12) and (3.13). To see when this could happen we first find the time it takes for the very first characteristics to meet by setting $\alpha \to 0^+$ in (3.8a). Without loss of generality, we make the assumption $V \geq 0, \gamma \leq 0$ henceforth. When the initial shear strain is zero, we have $\hat{\psi}(0) = \psi(0)$, yielding

$$t^0_\infty = \lim_{\alpha\to 0^+} \frac{\hat{\psi}(\alpha)}{V'(\alpha)} = -\, c_s^2 \lim_{\substack{\alpha\to 0^+\\ \gamma\to 0^-}} \left(V'(\alpha)\frac{\mathrm{d}c}{\mathrm{d}\gamma}\right)^{-1} \tag{3.25}$$

where we have used $(3.8a)^{2,3}$ and (2.12). Since $\frac{\mathrm{d}c}{\mathrm{d}\gamma}$ is bounded near zero shear strain, the only way for a shock to immediately form is when the initial loading rate, $V'(0)$, is infinite. However, this condition alone is insufficient, since for common materials the slope $\frac{\mathrm{d}c}{\mathrm{d}\gamma} \to 0$ may balance the loading singularity, leading to $t^0_\infty > 0$, as seen by examining the above equation. The distance at which the very first characteristics meet is given, using (3.6), as

$$X^0_\infty = c_s t^0_\infty \tag{3.26}$$

The time taken for the very first characteristics to realize an acceleration magnification M, and the distance at which it is realized, are similarly given by setting $\alpha \to 0^+$ in (3.22a) and (3.22b)

$$t^0_M = \lambda_M \lim_{\alpha\to 0^+} \frac{\hat{\psi}(\alpha)}{V'(\alpha)} = -\, c_s^2 \lambda_M \lim_{\substack{\alpha\to 0^+\\ \gamma\to 0^-}} \left(V'(\alpha)\frac{\mathrm{d}c}{\mathrm{d}\gamma}\right)^{-1} \quad , \quad X^0_M = c_s t^0_M \tag{3.27}$$

It can be seen from (3.25) and (3.27) that when the very first characteristics meet immediately ($t^0_\infty = 0$), any acceleration magnification $M \geq 1$ is also immediately realized ($t^0_M = t_M = 0$).

3.5 Solution for a general family of loadings

Our goal is to study the effect of material behaviour and the loading waveform on the shock evolution. To that end, we choose a general loading profile

$$V(t) = V_0 \begin{cases} \left(\dfrac{t}{t_0}\right)^n & 0 \leq t \leq t_0 \\ 1 & t \geq t_0 \end{cases} \tag{3.28}$$

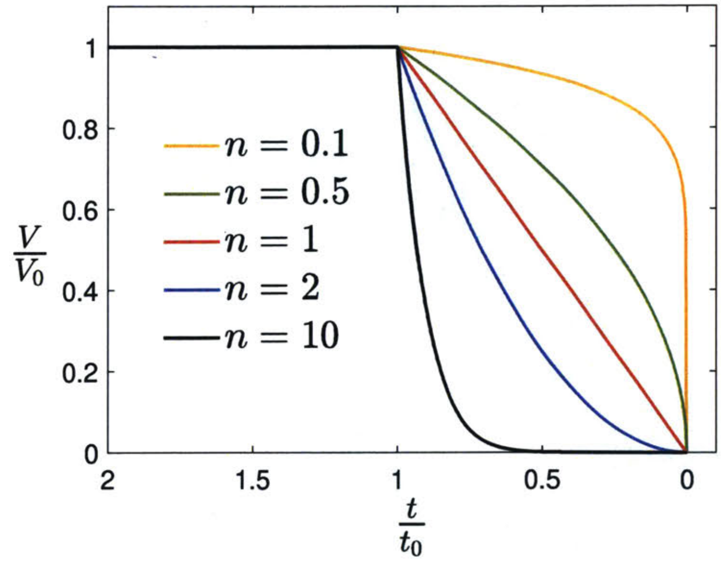

Figure 3-2: Family of loading profiles described by (3.28), V_0 is the ramp velocity, t_0 is the ramp time and n is the loading exponent. The initial loading rate is infinite for $n < 1$.

wherein the shearing velocity is ramped up in a continuous and monotonous fashion from zero at $t = 0$ to a ramp velocity V_0 within a ramp time t_0, after which the velocity is held constant. Different values of the loading exponent $n > 0$ reflect different ramping forms, as shown in Fig. 3-2, and in particular, $n = 1$ corresponds to linear ramping where the acceleration is constant during the ramping phase. Note that as discussed earlier in Sec. 3.3, an infinite initial loading rate ($t = 0$, $n < 1$) is not an evolved shock.

For the loading (3.28), using (3.2a) and (3.2b), the velocity and strain fields can be seen to be constant for characteristics $\alpha > t_0$ and thus the characteristics are parallel and there is no magnification in acceleration along charactersitics $\alpha > t_0$ (setting $V'(\alpha) = 0$ in (3.22a) gives $t_M^\alpha \to \infty$ for $t > t_0$ and $M > 1$). Thus we can restrict the minimisation in (3.20) and (3.22) to the ramping phase

$$t_M = \min_{\alpha \in [0,t_0]} \alpha + \lambda_M \frac{\hat{\psi}}{V'(\alpha)} \quad , \quad \alpha_{\min}^M = \arg\min_{\alpha \in [0,t_0]} t_M^\alpha \tag{3.29}$$

Henceforth, unless mentioned otherwise, we consider $\alpha \in [0, t_0]$. The loading is smooth in the interval of interest and hence, as discussed in Sec. 3.2, X_{shock} is also the shortest distance from the loading surface where characteristics intersect (assuming smooth material response). Using (3.2b), we can specialize (3.22b) for the loading (3.28) as (see Appendix A.1)

$$X_M = \frac{t_0 \lambda_M}{n V_0^{\frac{1}{n}}} \left. \frac{\psi c}{(-Q(\gamma))^{\frac{n-1}{n}}} \right|_{\gamma^M_{\text{min}}} \quad , \quad \gamma^M_{\text{min}} = \hat{\gamma}(\alpha^M_{\text{min}}) \tag{3.30}$$

The time t^0_M at which the very first characteristics attain acceleration magnification M, from (3.27), can be specialised for the loading (3.28) as (see Appendix A.1)

$$t^0_M = \frac{c_s^{1+\frac{1}{n}} t_0 \lambda_M}{n V_0^{1/n}} \lim_{\gamma \to 0^-} -\left(\frac{\mathrm{d}c}{\mathrm{d}\gamma}\right)^{-1} (-\gamma)^{\frac{1-n}{n}} \tag{3.31}$$

If p_0 is the order of the Taylor expansion of $\frac{\mathrm{d}c}{\mathrm{d}\gamma}$ for $\gamma \to 0^-$, i.e if

$$\left. \frac{\mathrm{d}c}{\mathrm{d}\gamma} \right|_{\gamma \to 0^-} \to -c_0(-\gamma)^{p_0} \tag{3.32}$$

where c_0 and p_0 are constants[3], then using (3.32) in (3.31) yields

$$t^0_M = \frac{c_s^{1+\frac{1}{n}} t_0 \lambda_M}{n c_0 V_0^{1/n}} (-\gamma)^{\frac{1}{n}-1-p_0} \tag{3.33}$$

We can define a critical loading exponent, denoted by $n_c (\leq 1)$,

$$n_c = \frac{1}{1 + p_0} \tag{3.34}$$

so that for $n < n_c$, we have $t^0_M = X_M = 0$ (using (3.33) and $(3.27)^2$), i.e there exists a material nonlinearity dependent loading exponent below which a shock forms immediately irrespective of the ramp velocity and ramp time. For $n > n_c$, we have $t^0_M, X^0_M \to \infty$ (using (3.34) in (3.33), $(3.27)^2$), that is the initial characteristics are parallel and there is no acceleration magnification along them (there will still be acceleration magnification and shock formation along later characteristics). For $n = n_c$, the values of t_M^0 and X_M^0 are finite and given by

---

[3] $c_0 > 0$ for a shock to form and $p_0 \geq 0$ since physically in the linear elastic limit we expect $|\frac{\mathrm{d}c}{\mathrm{d}\gamma}|$ to be bounded.

$$t_M^0\bigg|_{n=n_c} = \frac{c_s^{2+p_0}\ t_0\lambda_M(1+p_0)}{c_0 V_0^{1+p_0}} \quad , \quad X_M^0\bigg|_{n=n_c} = \frac{c_s^{3+p_0}\ t_0\lambda_M(1+p_0)}{c_0 V_0^{1+p_0}} \tag{3.35}$$

Essentially from (3.27), t_M^0 and X_M^0 are inversely proportional to the limit of the product $V'(\alpha)\frac{\mathrm{d}c}{\mathrm{d}\gamma}$ near zero strain and thus there is a competition between the loading rate and the material's ability to resist nonlinear evolution decided by $|\frac{\mathrm{d}c}{\mathrm{d}\gamma}|$ (the smaller it is the less nonlinear the shear response and the easier it is for the material to relay the waveform as a spatially smooth one). For $n < n_c$, the loading rate singularity immediately overpowers the material's ability to resist shock formation (resisting characteristics intersecting / acceleration magnification limit from becoming infinite). The weaker the nonlinearity, the higher the p_0 (from (3.32)) and thus smaller the n_c using (3.34), meaning more powerful/singular loadings ($n < n_c$) are required to immediately form shocks for materials with weaker nonlinearity.

An essential function required for the minimisation in (3.29) is the derivative $\frac{\mathrm{d}t_M^\alpha}{\mathrm{d}\alpha}$, which for the loading (3.28) can be written as below (see Appendix A.2 for derivation),

$$\frac{\mathrm{d}t_M^\alpha}{\mathrm{d}\alpha} = \hat{G}(\alpha) = 1 + \hat{R}\lambda_M + \frac{\hat{\psi}(n-1)\lambda_M}{\hat{Q}n} \quad , \quad R(\gamma) = -\frac{\mathrm{d}\psi}{\mathrm{d}\gamma}c^{-1} \tag{3.36}$$

In the next Chapter, we will apply the formulas developed here to investigate transient evolution of shear waves into shocks for materials with different constitutive responses.

Chapter 4

Analysis for different nonlinear shear constitutive responses

In this Chapter, we will use the formulas developed in Chapter 3 to investigate transient evolution of shear waves into shocks for materials with different constitutive responses. The Gent (Gent, 1996) and Ogden (Ogden, 1972) models are widely used for modelling the response of soft solids. We first use an exponential stress model which is not derived from any hyperelastic strain energy, but is one that greatly simplifies the analysis, and different features of the results therein carry over to the Gent and two parameter Ogden hyperelastic models (for parameter values that predict stiffening) analyzed subsequently. We apply the results of our analysis to a physical problem of shear impact of the brain in Chapter 5.

4.1 Exponential stress model

A simple function for the shear response that captures the nonlinear strain stiffening reported in experiments and allows for easy analytical tractability for our problem, is an exponential stress-strain response of the form

$$\tau(\gamma) = \frac{\mu}{k}(e^{k|\gamma|} - 1)\mathrm{sign}(\gamma) \tag{4.1}$$

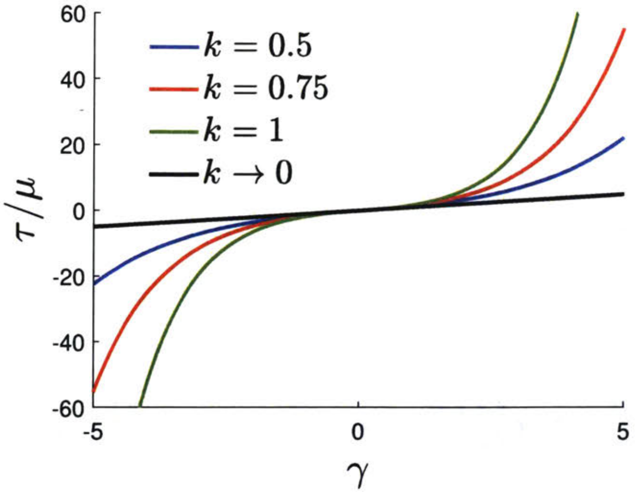

(a) Plot of the dimensionless shear stress as a function of the shear strain γ.

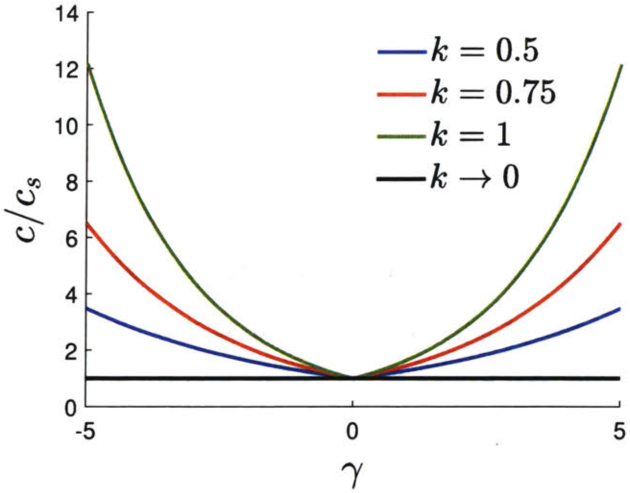

(b) Plot of the dimensionless shear wavespeed as a function of the shear strain γ.

Figure 4-1: Exponential stress model (4.1). The $k \to 0$ limit reduces to a Neo-Hookean shear response and $\gamma \to 0$ for any k captures the linear elastic stress strain response.

where $k > 0$ is a dimensionless parameter that quantifies the nonlinear stiffening. This function reduces to a linear elastic response in the limit of $\gamma \to 0$. However, it is not derived from any established hyperelastic strain energy function and is simply being used as a phenomenological model for analytical tractability; many features of the results carry over to the analysis for Gent and two parameter Ogden hyperelastic models in the subsequent sections. For the response (4.1), we have $\tau''(|\gamma|) > 0$ and hence shocks will be formed in loading. Using (2.11), the wavespeed is given by

$$c(\gamma) = c_s e^{\frac{k}{2}|\gamma|} \tag{4.2}$$

Fig. 4-1 shows plots of the stress response and the shear wavespeed for different values of the stiffening parameter k.

The derivative of the wavespeed is given by

$$\frac{\mathrm{d}c}{\mathrm{d}\gamma} = \frac{c_s k}{2} e^{\frac{k}{2}|\gamma|} \mathrm{sign}(\gamma) \quad \text{for} \quad \gamma \neq 0 \tag{4.3}$$

Thus from (3.32), we have $p_0 = 0$ and $c_0 = c_s k/2$ for (4.3), and using (3.34) we get $n_c = 1$. Thus, for $n < 1$, we have $t_{\text{shock}} = t_M = 0$ and $X_{\text{shock}} = X_M = 0$. This is not an artifact of the initial loading rate being infinite for $n < 1$ but instead represents the limit of acceleration magnification becoming infinite. In the subsequent sections for Gent and Ogden solids it will be shown that an infinite initial loading rate can still require a finite time and distance for the magnification in acceleration to increase or become infinite. Note that this deviation from conventional hyperelastic models essentially stems from the sign(γ) factor in the stress response that allows for a quadratic term in the stress expansion whereas conventional hyperelastic models would only allow a cubic term. For $n \geq 1$ we have to perform the minimization in $(3.29)^2$ to find α^M_{min}.

Further, we write,

$$Q(\gamma) = V_*(e^{\frac{k}{2}|\gamma|} - 1)\mathrm{sign}(\gamma) \quad \text{where} \quad V_* = \frac{2c_s}{k} \tag{4.4}$$

where we define a characteristic scaling velocity V_* (not to be confused with velocity of a characterisitic). As mentioned earlier we assume $V \geq 0$, $\gamma \leq 0$. Using (3.2b), we have

$$\gamma = -Q^{-1}(V(\alpha)) = -\frac{2}{k} \ln\left(1 + \frac{V}{V_*}\right) \tag{4.5}$$

Using (4.5), we have for the exponential solid (refer Appendix A.3.1)

$$\hat{c} = c_s\left(1 + \frac{V}{V_*}\right) \quad , \quad \hat{\psi} = V + V_* \quad , \quad \hat{R} = 1 \tag{4.6}$$

Combining eqs (3.36), (4.6) and (3.2b) we have

$$\frac{\mathrm{d}t_M^\alpha}{\mathrm{d}\alpha} = 1 + \lambda_M - \frac{(n-1)\lambda_M}{n}\left(1 + \frac{V_*}{V}\right) \tag{4.7}$$

For $n = n_c = 1$ we have $\frac{\mathrm{d}t_M^\alpha}{\mathrm{d}\alpha} > 0$ and thus $\alpha_{\min}^M = 0$. Acceleration magnification and shock formation thus initiate at the leading edge of the waveform for $n = n_c$ and using (3.21) and $(3.35)^2$ we have

$$X_M = X_M^\alpha\Big|_{\alpha_{\min}^M} = X_M^0\Big|_{n=n_c} = \frac{2c_s^2\, t_0\lambda_M}{kV_0} = \frac{L_*\lambda_M}{m} \tag{4.8}$$

where we define the loading mach number $m(\geq 0)$ and the characteristic length scale L_* as

$$m = \frac{V_0}{V_*} \quad , \quad L_* = c_s t_0 \tag{4.9}$$

Using (4.7) to perform the minimization in $(3.29)^2$ for $n > 1$, we end up with (see Appendix A.3.1)

$$\alpha_{\min}^M = \begin{cases} t_0\left(\dfrac{m_{\text{th}}}{m}\right)^{\frac{1}{n}} & n > 1,\ m \geq m_{\text{th}} \\[2ex] t_0 & n > 1,\ 0 \leq m < m_{\text{th}} \end{cases} \tag{4.10}$$

where we have defined the the threshold mach number m_{th} as

$$m_{\text{th}} = \frac{(n-1)\lambda_M}{n + \lambda_M} \quad (n > 1) \quad , \quad 0 < m_{\text{th}} < \lambda_M(< 1) \tag{4.11}$$

The threshold mach number is an increasing function of both the loading exponent n and the target acceleration magnification $M(= 1 - 1/\lambda_M)$. Additionally, $m_{\text{th}} \to 0$ as $n \to 1$. From (4.10), we see that for loadings with $n > 1$, the earliest realization of target acceleration magnification or shocks can happen either at the the trailing edge of the waveform ($\alpha = t_0$) or in the ramping part ($0 < \alpha < t_0$) depending on m and m_{th}.

Using (4.10) in (3.22b), and the result (4.8), we have X_M, the location where an acceleration magnification of M is realized earliest in the solid, non-dimensionalized by L_* as (see Appendix A.3.1)

$$\frac{X_M}{L_*} = \begin{cases} 0 & n < 1,\ m \geq 0 \\ \dfrac{\lambda_M}{m} & n = 1,\ m \geq 0 \\ \dfrac{n(1+\lambda_M)^2}{(n-1)(n+\lambda_M)}\left(\dfrac{m_{\text{th}}}{m}\right)^{\frac{1}{n}} & n > 1,\ m \geq m_{\text{th}} \\ \dfrac{\lambda_M}{n}\left(2 + m + \dfrac{1}{m}\right) & n > 1,\ 0 \leq m < m_{\text{th}} \end{cases} \tag{4.12}$$

The solution is continuous at $n \to 1^+$ and at $m \to m_{\text{th}}^-$ but is discontinuous at $n \to 1^-$ (see Appendix A.3.1). Setting $M \to \infty$, that is $\lambda_M = 1$, in (4.12) gives the non-dimensionalized shock location,

$$\frac{X_{\textbf{shock}}}{L_*} = \begin{cases} 0 & n < 1,\ m \geq 0 \\ \dfrac{1}{m} & n = 1,\ m \geq 0 \\ \dfrac{4n}{n^2-1}\left(\dfrac{m_{\text{th}}}{m}\right)^{\frac{1}{n}} & n > 1,\ m \geq m_{\text{th}} \\ \dfrac{1}{n}\left(2 + m + \dfrac{1}{m}\right) & n > 1,\ 0 \leq m < m_{\text{th}} \end{cases} \tag{4.13}$$

where $m_{\text{th}} = (n-1)/(n+1)$. The expressions in (4.12) and (4.13) provide us the location of first realization of given acceleration magnification and of first shock formation respectively.

Non-dimensional maps: The result in eq. (4.13) allows us to make non-dimensional phase maps, such as the representative one shown in Fig. 4-2(a) for

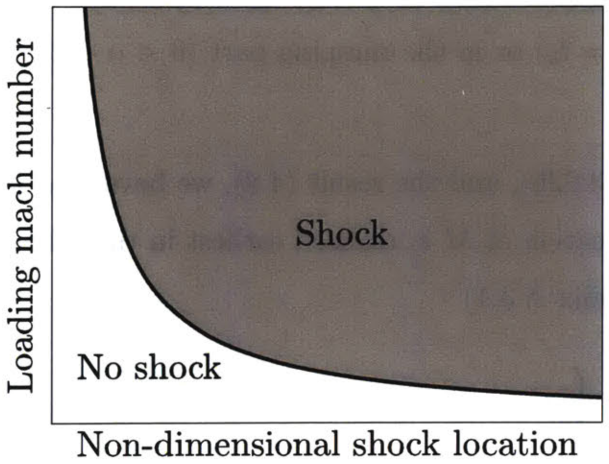

(a) Representative non-dimensional phase map of the shock location for a given loading exponent $n \geq n_c$.

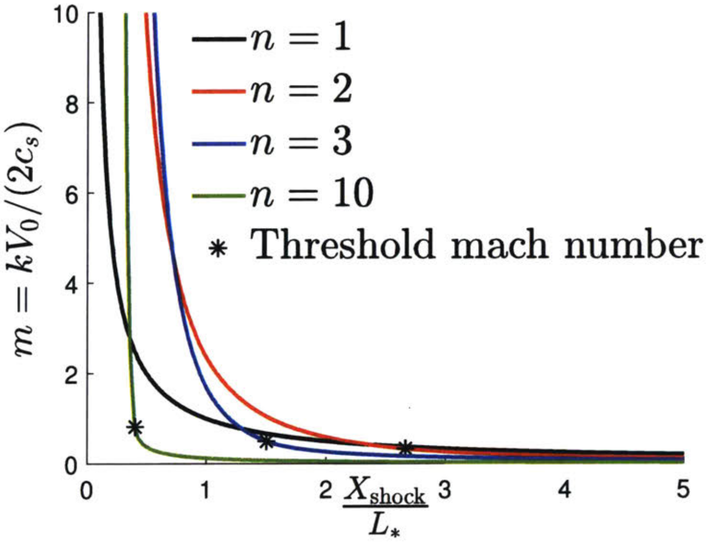

(b) Non-dimensional maps of shock location as a function of the loading mach number m, for various loading exponents, using the result (4.13) for the exponential stress model (4.1). For $n > 1 (n_c)$, a threshold mach number (m_{th}) separates two different functional forms of X_{shock}/L_*. In different loading mach number regimes different loading exponents might delay shock formation.

Figure 4-2: Non-dimensional maps of shock location.

a given loading exponent $n \geq n_c$, that would allow us to determine whether or not a shock would form within a given distance from the loading surface. The maps can serve as a guide in design problems. For example, they can be used to estimate the maximum length one could design for, while avoiding shock formation for a given material and loading[1]. Similarly they can be used to design loadings that will avoid shock formation given a material and a length scale, or to choose a material that will avoid shocks within a given length scale for a given loading. In Fig. 4-2(b), we use (4.13) to make such maps for different values of the loading exponent n, where we have the loading mach number $m = kV_0/(2c_s)$ on the vertical axis and the distance for first shock formation non-dimensionalized by $L_* = c_s t_0$ on the horizontal axis. We can see that X_{shock}/L_* reduces with increasing loading mach number for any n (can be shown for any $n \geq 1$ from (4.13)). For $n > 1(n_c)$ there is a threshold mach number separating different functional forms of X_{shock}.

Effect of material parameters: We first fix the loading waveform and study the effect of material parameters on shock evolution. The material response is quantified by the nonlinearity parameter k, which influences the loading mach number m, and by the linear elastic shear modulus μ, which appears through c_s in both m and L_*. Since X_{shock} reduces with increasing m and reducing L_*, higher material nonlinearity (higher k) and lower μ reduce the distance taken for first shock formation.

Effect of loading: Next, we fix the material properties and analyze the effect of the loading parameters. The loading mach number m increases with V_0 and hence, a higher ramp velocity reduces X_{shock} (for a fixed n and t_0). The ramp time t_0 enters through $L_* = c_s t_0$, and thus X_{shock} scales linearly with t_0 for given V_0 and n. Thus as $t_0 \rightarrow 0$, we have $X_{\text{shock}} \rightarrow 0$, i.e as the loading waveform approaches a discontinuity, a pure shock is immediately formed. The loading exponent n seems to have the most profound and non-trivial effect on shock evolution. For example, it can be seen that going from $n \rightarrow 1^-$ to $n = 1(n_c)$ may be the difference between a shock immediately forming versus at a distance L_*/m (see (4.13)). From Fig. 4-2(b), it can be seen that at a given loading mach number the trend in first shock location with respect to the loading exponent is non-monotonous. Also, the maps for different loading exponents intersect each other, meaning that there are different loading mach number regimes in which different loading exponents could delay shock formation. This could have implications for design of protective structures, if we know the mach regime we are

---

[1] Neglecting reflections in a finite dimensional system.

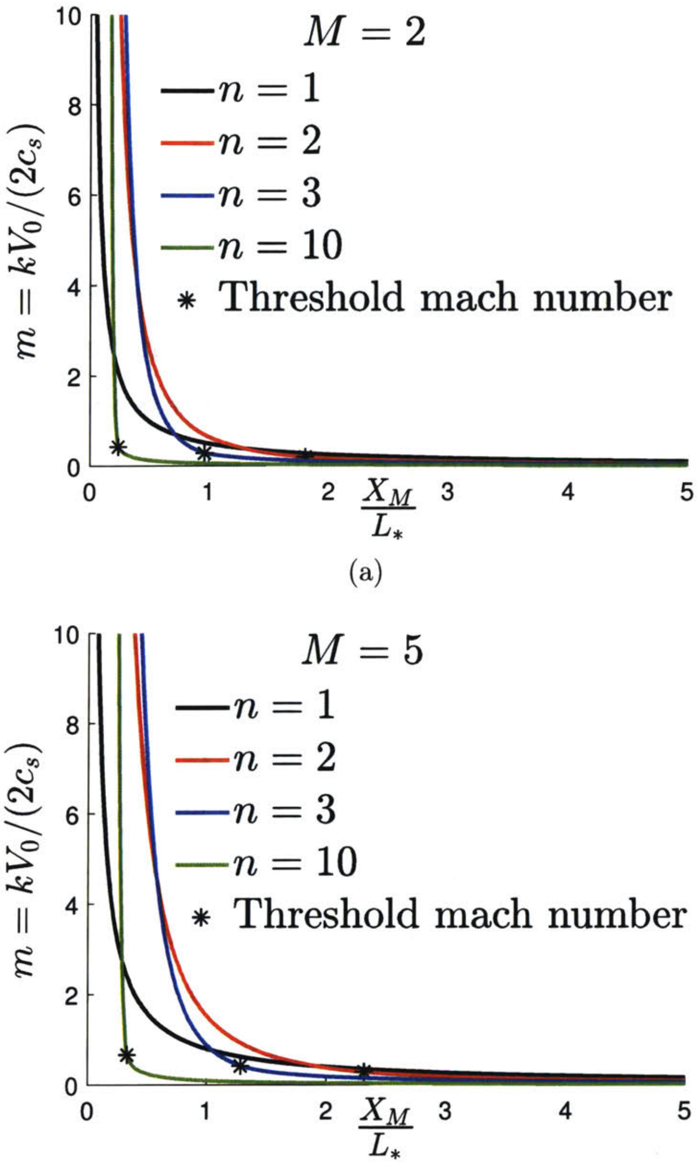

(a)

(b)

Figure 4-3: Exponential stress model (4.1): Maps of the dimensionless distance of first realization of acceleration magnification M, for varying loading mach number m and different loading exponents n, using (4.12).

operating in for a given problem, we can select a target waveform (by choosing n) that could delay the shock formation.

Acceleration magnification: Using (4.12) we can make non-dimensional maps as shown in Figs. 4-3-4-4, where we have the loading mach number on the vertical axis and the location of first realization of a given acceleration magnification M, non-

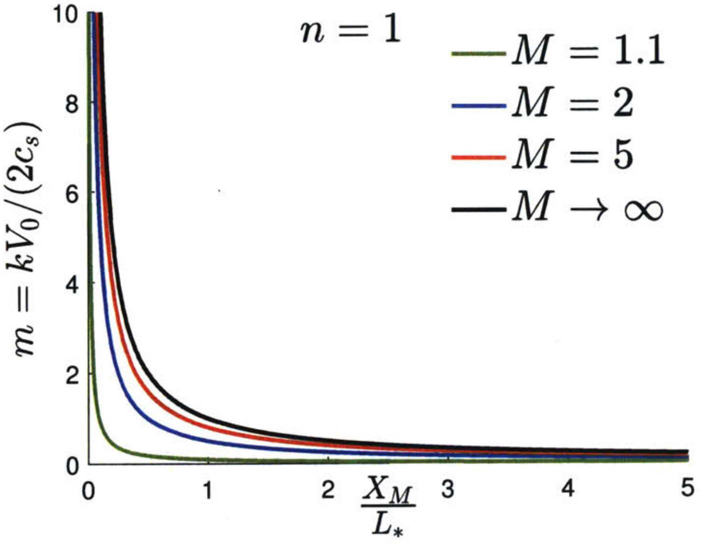

(a) Maps at different M for $n = 1(n_c)$.

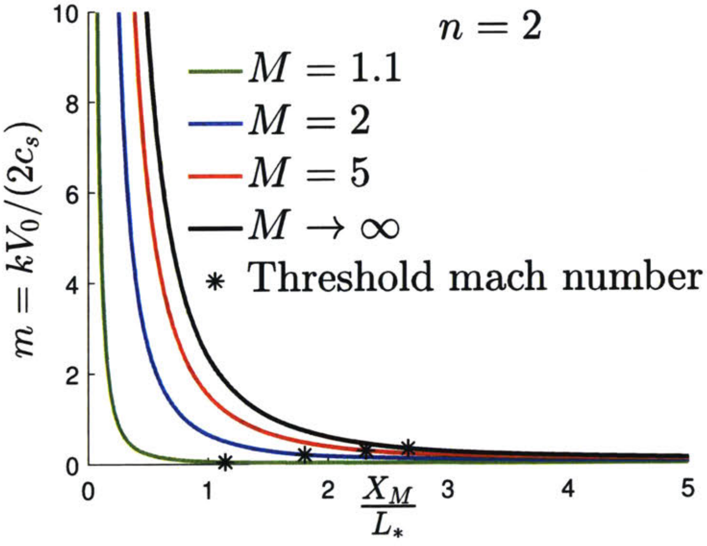

(b) Maps at different M for $n = 2$.

Figure 4-4: Exponential stress model (4.1): Maps of the dimensionless distance of first realization of acceleration magnification M, for varying loading mach number m, using (4.12). Curves for X_M quickly converge to that of the shock location ($M \to \infty$) at higher values of M.

dimensionalized by L_* on the horizontal axis. From Fig. 4-3, it can be seen that X_M shows a similar qualitative dependence on the material and loading parameters as X_{shock} and the commentary for shock formation carries over. However, when $n > 1(n_c)$ and $m > m_{\text{th}}$, the distance at which a given finite acceleration magnification is realized earliest in time need not be the shortest distance at which it is achieved (see Appendix A.3.1). In Fig. 4-4, we have maps of X_M/L_* for two different loading exponents and a range of increasing M, the limit $M \to \infty$ corresponds to X_{shock}/L_*. For a given material and loading it takes longer distances for first realization of higher acceleration magnifications, as one would expect. More importantly, it can be seen that the evolution from high acceleration magnifications ($M \sim 5$) to a shock wave ($M \to \infty$) happens over much shorter distances than the distance taken for realization of those high acceleration magnifications (starting from $M = 1$). This is true for any $n \geq 1(n_c)$ though only two loading exponents have been shown here. If the ramping is linear ($n = 1$) so that the acceleration imposed at the loading surface is constant during ramping, maps in Fig. 4-4(a) can also be used to predict the maximum acceleration realized within a length scale[2]. This might be useful for application to biological systems where the damage tolerance might be quantified in terms of maximum acceleration.

Post first shock formation: Note that we have restricted our discussion so far to the onset of shock formation and have not touched on the strength of the shock. The first shock that forms would be weak, with the jump in velocity and strain fields being small. Assuming a steady state pure shock ultimately propagates into the material, the weak initial shock would eventually grow into a stronger shock with a jump in velocity from 0 to V_0 across the shock, and this would happen over longer distances for materials with weaker nonlinearity of shear response. The strength of the steady state shock would be higher for higher ramp velocity V_0 and a consideration of the shock strength would be pertinent for materials with viscosity as it would be tougher to dissipate away larger discontinuities. Post the first shock formation we would have to apply the integral form of balance laws in a small volume surrounding the shock while using (2.17) in the smooth regions, however $f(\beta)$ (from (2.17)) will no longer be constant behind the shock and there will be information travelling along negative X_2 direction as well (see Appendix B for a relevant discussion). The problem becomes analytically intractable post shock initiation and would have to be studied numerically wherein numerical viscosity effects are inevitable.

---

[2] Neglecting reflections in a finite dimensional system.

4.2 Gent model

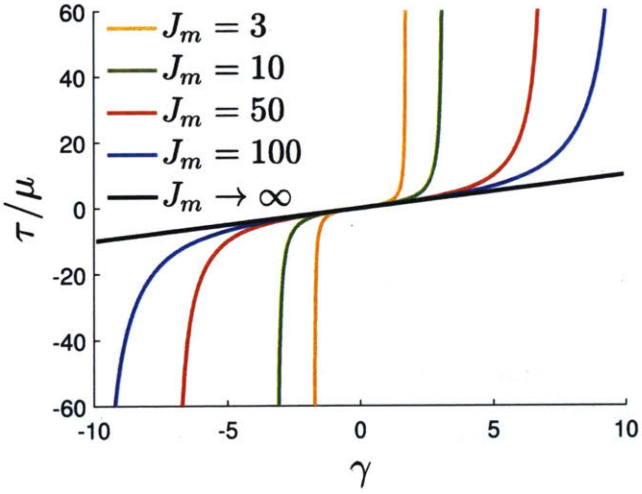

(a) Plot of the dimensionless shear stress as a function of the shear strain γ.

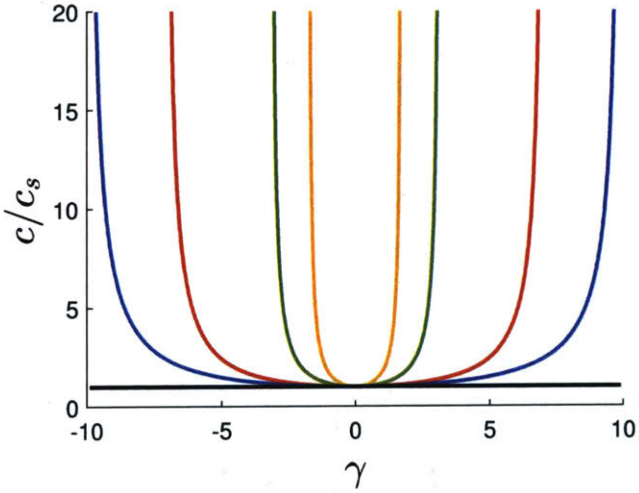

(b) Plot of the dimensionless shear wavespeed (same plot legend as for (a)) as a function of the shear strain γ.

Figure 4-5: Gent model (4.15). The stresses and wavespeeds become unbounded as the magnitude of shear strains approach the locking limit $\sqrt{J_m}$. Smaller the J_m, the more nonlinear the shear response of the solid.

The popular and widely used Gent hyperelastic model (Gent, 1996) is based on the concept of limiting chain extensibility where the strain energy density function is designed to have a singularity when the first invariant of $\mathbf{B}$, reaches a limiting value

$I_m = J_m + 3$,

$$W = -\frac{\mu J_m}{2}\ln\left(1 - \frac{I_1 - 3}{J_m}\right) \tag{4.14}$$

For the simple shear deformation (2.4), this translates to limiting the magnitude of shear strain to a locking strain of $\gamma_m = \sqrt{J_m}$ as the shear stress keeps increasing (using (4.14) in (2.7)),

$$\tau(\gamma) = \frac{\mu J_m \gamma}{J_m - \gamma^2} \quad \text{where} \quad J_m = \gamma_m^2 \tag{4.15}$$

Plots of the shear stress-strain curves for various values of J_m are shown in Fig. 4-5(a), the smaller the J_m the more nonlinear the shear response. When $J_m \to \infty$, the strain energy density function in (4.14) reduces to that of the neo-Hookean solid, yielding a linear shear stress-strain response. For finite J_m, we have $\tau''(|\gamma|) > 0$ and hence, a solid whose shear response is well modelled by the Gent model will produce shear shocks in loading. We define a fractional shear strain δ which is the ratio of the shear strain and the locking strain γ_m,

$$\delta = \frac{\gamma}{\gamma_m} = \frac{\gamma}{\sqrt{J_m}} \quad , \quad |\delta| < 1 \tag{4.16}$$

Once again, without loss of generality we assume $V \geq 0$ and thus $\gamma, \delta \leq 0$. Functions of the shear strain $f(\gamma)$ can be written as $\tilde{f}(\delta) = f(\delta\sqrt{J_m})$ where the tilde superscript denotes that the argument of the function is δ. Using (2.11), the wavespeed for the stress response (4.15) is given by

$$c(\gamma) = V_*\frac{\sqrt{J_m + \gamma^2}}{J_m - \gamma^2} \quad \text{where} \quad V_* = c_s\sqrt{J_m} \quad ; \quad \tilde{c}(\delta) = c_s\frac{\sqrt{1 + \delta^2}}{1 - \delta^2} \tag{4.17}$$

Here, as in (4.4), we have defined a stiffening parameter dependent characteristic scaling velocity V_*. Plots of the wavespeed as a function of the shear strain are showin in Fig 4-5(b) for various values of J_m. All of these curves collapse onto a single curve when plotted as a function of δ as shown in Fig. 4-6. We can also write

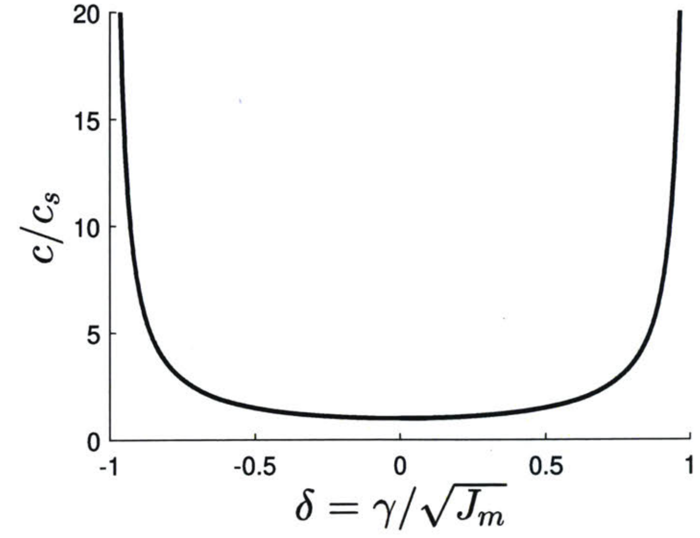

Figure 4-6: Gent model (4.15): Plot of the dimensionless wavespeed as a function of the fractional shear strain $\delta = \gamma/\sqrt{J_m}$, using (4.17).

(3.2b) in terms of the fractional shear strain,

$$\tilde{Q}(\delta) = -V(\alpha) \tag{4.18}$$

For the Gent stress response (4.15), we have

$$\tilde{Q}(\delta) = V_* \log\left(\frac{\left(\frac{\sqrt{1+\delta^2}+\delta\sqrt{2}}{\sqrt{1+\delta^2}-\delta\sqrt{2}}\right)^{\frac{1}{\sqrt{2}}}}{\delta+\sqrt{1+\delta^2}}\right) \tag{4.19}$$

where $\tilde{Q}$ is an odd function. We can divide (4.18) and (4.19) by V_* to write

$$\tilde{q}(\delta) = \frac{\tilde{Q}(\delta)}{V_*} = -\frac{V}{V_*} \quad \Rightarrow \quad \delta = -\tilde{q}^{-1}\left(\frac{V}{V_*}\right) \quad \text{where} \quad \tilde{q}(\delta) = \log\left(\frac{\left(\frac{\sqrt{1+\delta^2}+\delta\sqrt{2}}{\sqrt{1+\delta^2}-\delta\sqrt{2}}\right)^{\frac{1}{\sqrt{2}}}}{\delta+\sqrt{1+\delta^2}}\right) \tag{4.20}$$

where $|\tilde{q}(\delta)|$ can be thought of as the local mach number dependent on the local velocity field $V(\alpha(X_2, t))$ (different from the loading mach number m which depends on ramp velocity V_0 and is constant for a given loading). Equation (4.18) provides a mapping $\delta = \hat{\delta}(\alpha)$, allowing us to switch function arguments between δ or α i.e $\hat{F}(\alpha) = \tilde{F}(\hat{\delta}(\alpha))$. Thus, we can rewrite (3.30) as

$$X_M = \frac{t_0 \lambda_M}{n V_0^{\frac{1}{n}}} \left. \frac{\tilde{\psi}\tilde{c}}{(-\tilde{Q}(\delta))^{\frac{n-1}{n}}} \right|_{\delta^M_{\text{min}}} \quad \text{where} \quad \delta^M_{\text{min}} = \hat{\delta}(\alpha^M_{\text{min}}) \tag{4.21}$$

which can be evaluated further for the Gent solid as (see Appendix A.3.2)

$$X_M = \frac{L_* \lambda_M}{n m^{\frac{1}{n}}} \left. \frac{K(\delta)}{(-q(\delta))^{\frac{n-1}{n}}} \right|_{\delta^M_{\text{min}}} \quad , \quad K(\delta) = \frac{-\,(1+\delta^2)^2}{\delta(3+\delta^2)(1-\delta^2)} \tag{4.22}$$

The loading mach number m and characteristic length scale L_* are defined in (4.9).

The derivative of the wavespeed (4.17) is given by

$$\frac{\mathrm{d}c(\gamma)}{\mathrm{d}\gamma} = \frac{V_* \gamma (3J_m + \gamma^2)}{(J_m - \gamma^2)^2 \sqrt{J_m + \gamma^2}} \quad , \quad \frac{\mathrm{d}c(\gamma)}{\mathrm{d}\gamma} \to \frac{3c_s \gamma}{J_m} \quad \text{as} \quad \gamma \to 0^- \tag{4.23}$$

Thus, from (3.32), $p_0 = 1, c_0 = 3c_s/J_m$ for (4.23), and from (3.34) we have the value of critical loading exponent as $n_c = 0.5$. Thus, for a Gent solid, even though the initial loading rate is infinite for $0.5 < n < 1$, the limit of acceleration magnification does not become infinite immediately. It does however for $n < 0.5$. For loading exponent values $n \geq 0.5$, we have to perform the minimization (3.20) to find α^M_{min} needed in (4.21). Writing the different functions in terms of fractional strain δ and then plugging them into (3.36) we end up with (see Appendix A.3.2)

$$\frac{\mathrm{d}t^\alpha_M}{\mathrm{d}\alpha} = \tilde{G}(\delta) = 1 - \frac{3(1-\delta^2)^2 \lambda_M}{\delta^2 (3+\delta^2)^2} - \frac{(1+\delta^2)^{\frac{3}{2}}}{\delta(3+\delta^2)} \frac{(n-1)\lambda_M}{n \tilde{q}(\delta)} \quad 0 \leq |\delta| < 1 \tag{4.24}$$

For $n = 0.5(n_c)$, it can be shown that for $0 < |\delta| < 1$, the function $\tilde{G}(\delta)$ is positive and hence, $\alpha^M_{\text{min}} = \delta^M_{\text{min}} = 0$. Thus, acceleration magnification and shock formation initiates at the leading edge of the waveform once again for $n = n_c$, and using (3.21)

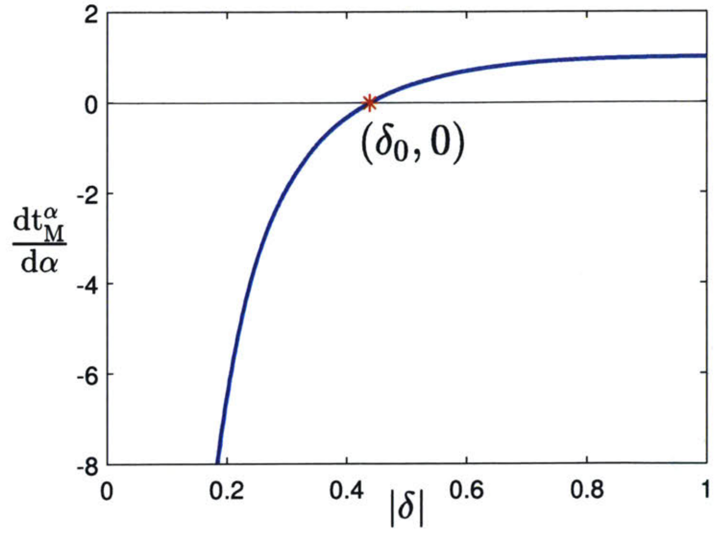

(a) Plot of $\frac{\mathrm{d}t_M^\alpha}{\mathrm{d}\alpha}$ versus the magnitude of the fractional shear strain for $\lambda_M, n = 1$ using (4.24). The nature of the plot remains the same for any $\lambda_M (= 1 - 1/M) \in (0, 1)$ and any $n > 0.5$, as $\delta \to 0^-$, the limit $\frac{\mathrm{d}t_M^\alpha}{\mathrm{d}\alpha} \to -\infty$ and $\frac{\mathrm{d}t_M^\alpha}{\mathrm{d}\alpha}$ changes sign from negative to positive at the root $|\hat{\delta}(\alpha)| = \delta_0$.

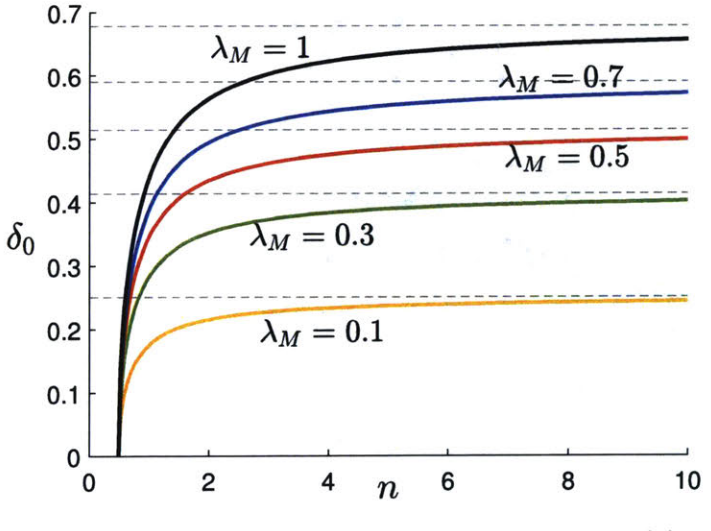

(b) Plots of δ_0 versus the loading exponent for different values of λ_M. The dotted lines represent the asymptotic value of δ_0 as $n \to \infty$ and $\delta_0 \to 0$ as $n \to 0.5$.

Figure 4-7: Gent model (4.15). Quantities related to the minimization of time taken for characteristics to meet.

and $(3.35)^2$ we have

$$X_M = X_M^\alpha\Big|_{\alpha_{\min}^M} = X_M^0\Big|_{n=n_c} = \frac{2c_s^3\, t_0 \lambda_M J_m}{3V_0^2} = \frac{2L_* \lambda_M}{3m^2} \tag{4.25}$$

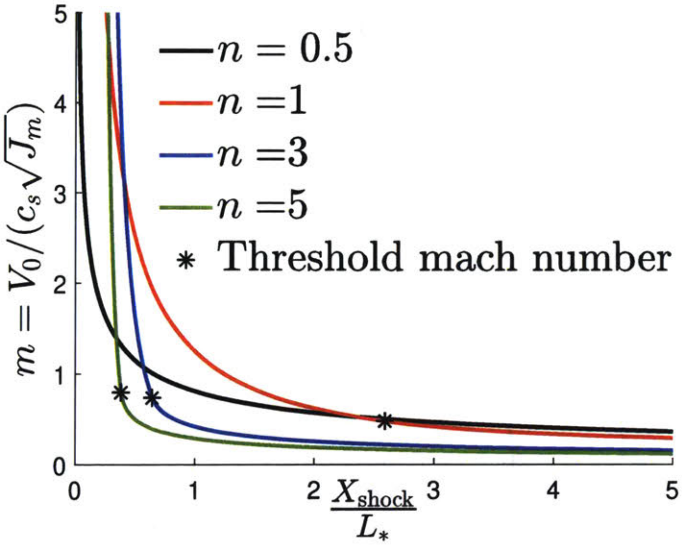

Figure 4-8: Gent model (4.15): Non-dimensional map of the shock location as a function of the loading mach number m, for various loading exponents (using $\lambda_M = 1$ in (4.27)). For $n > 0.5(n_c)$, a threshold mach number (m_{th}) separates two different functional forms of X_{shock}/L_*. In different loading mach number regimes different loading exponents might delay shock formation.

For $n > 0.5$, the plot of $\frac{\mathrm{d}t_M^{\alpha}}{\mathrm{d}\alpha}$ vs $|\delta|$ is qualitatively similar to the plot in Fig. 4-7(a), with a zero, $\delta_0 \in (0,1)$. That is, for $|\delta| < \delta_0$, the derivative $\frac{\mathrm{d}t_M^{\alpha}}{\mathrm{d}\alpha}$ is negative, for $|\delta| > \delta_0$, it is positive and is zero at $|\delta| = \delta_0$. Thus if the loading mach number is high enough such that a fractional shear strain magnitude of δ_0 is realized at the loading surface during the loading, then $\delta_{\min}^M$ will be[3] $-\delta_0$. We can evaluate the threshold mach number m_{th}, which is the minimum value of the loading mach number required to realize a fractional strain magnitude of δ_0 during loading, by setting $m_{\text{th}} = \tilde{q}(\delta_0)$ using (4.20) (note that $\delta_0 > 0$). When $m < m_{\text{th}}$, the loading is not high enough to generate fractional strain magnitudes greater than or equal to δ_0 and since $\frac{\mathrm{d}t_M^{\alpha}}{\mathrm{d}\alpha} < 0$ for $|\delta| < \delta_0$, the minimizer $\delta_{\min}^M$ would simply be the largest (in magnitude) fractional strain realized. This would correspond to the strain state at the end of ramping when

---

[3] Minus sign since $\delta_0 > 0$, $\delta_{\min}^M < 0$.

$|q|$ reaches m in (4.20). Thus,

$$\text{for } n > 0.5 \quad , \quad \delta_{\text{min}}^{M} = -\begin{cases} \delta_0 & m \geq m_{\text{th}}(=\tilde{q}(\delta_0)) \\ \tilde{q}^{-1}(m) & m < m_{\text{th}} \end{cases} \tag{4.26}$$

Hence, once again, for $n > n_c$, depending on the loading mach number and threshold mach number, earliest realization of a shock or given acceleration magnification can happen at the trailing edge ($\hat{\delta}(t_0) = -\tilde{q}^{-1}(m)$) or the middle of the ramping part of the waveform. Plots of δ_0 as a function of the loading exponent n for different values of λ_M are shown in Fig. 4-7(b), it can be seen that $\delta_0 \to 0$ as $n \to 0.5$. Also, δ_0 is higher for higher acceleration magnification for a given loading exponent $n > 0.5$, and for a given acceleration magnification, δ_0 is higher for higher n.

Plugging (4.26) into (4.22), and using the result (4.25), we obtain the solution for non dimensionalized X_M for Gent solids (see Appendix A.3.2),

$$\frac{X^M}{L^*} = \lambda_M \begin{cases} 0 & n < 0.5, \ m \geq 0 \\ \dfrac{2}{3m^2} & n = 0.5, \ m \geq 0 \\ \dfrac{K(-\delta_0(\lambda_M, n))}{n \ m^{\frac{1}{n}} \ m_{\text{th}}^{\frac{n-1}{n}}} & n > 0.5, \ m \geq m_{\text{th}} \\ \dfrac{K\big|_{-\tilde{q}^{-1}(m)}}{n \ m} & n > 0.5, \ 0 \leq m < m_{\text{th}} \end{cases} \tag{4.27}$$

where $m_{\text{th}} = \tilde{q}(\delta_0(\lambda_M, n))$ and $\delta_0(\lambda_M, n)$ is the positive root of $\tilde{G}(\delta)$ in (4.24). Setting $\lambda_M = 1$ gives the expressions for X_{shock}/L^* for the incompressible Gent hyperelastic solid. Once again it can be verified that the only discontinuity in the solution space is in moving from $n \to {n_c}^-$ to n_c (0.5 for Gent solid).

The results for a Gent solid are shown in Figs. 4-8-4-10 and can be seen to be exactly similar in nature to the results for the exponential stress model except the fact that n_c is now 0.5 instead of 1 and thus shocks are immediately formed for loadings

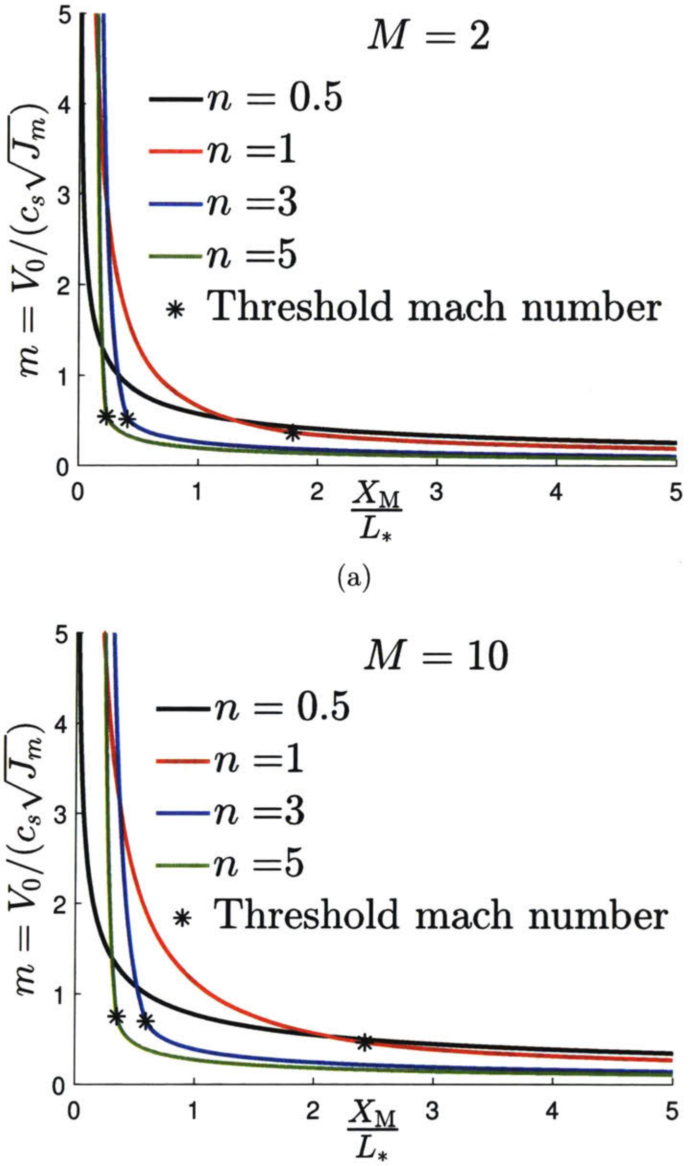

(a)

(b)

Figure 4-9: Gent model (4.15): Maps of the dimensionless distance of first realization of acceleration magnification M, for varying loading mach number m and different loading exponents n, using (4.27).

with loading exponent $n < 0.5$ and the threshold mach number separating different functional forms of the non-dimensional evolution distances comes in the picture for $n > 0.5$. Increasing material nonlinearity (lower J_m instead of higher k) once again hastens shock evolution and other observations made for the results of the exponential model carry over.

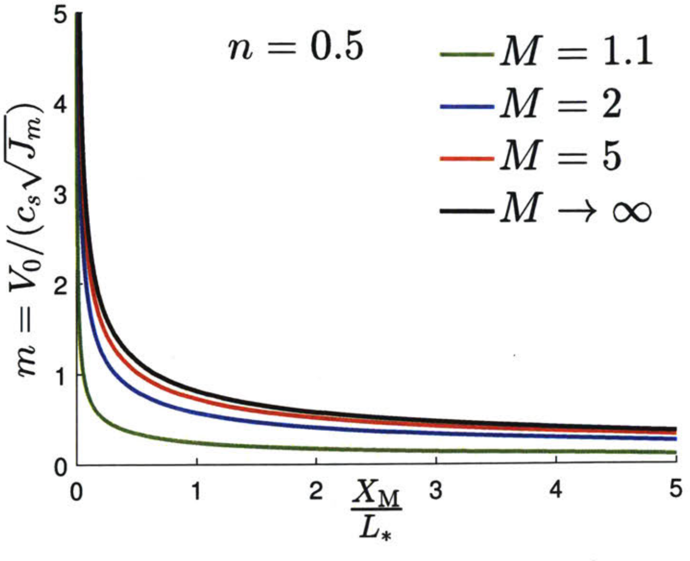

(a) Maps at different M for $n = 0.5(n_c)$.

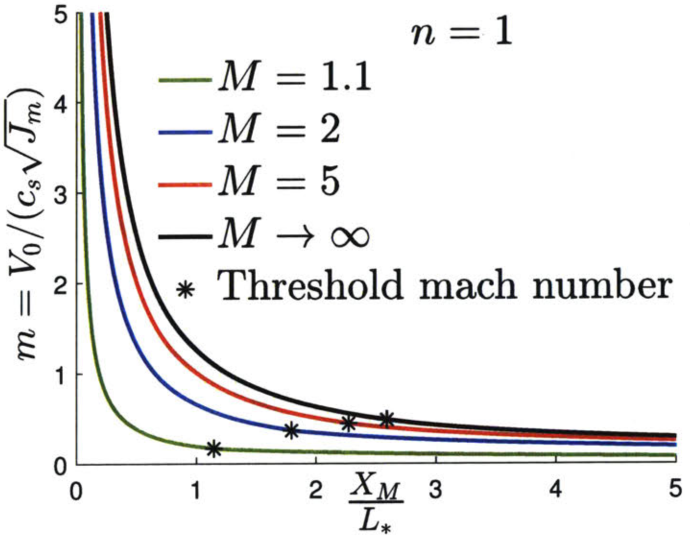

(b) Maps at different M for $n = 1$.

Figure 4-10: Gent model (4.15): Maps of the dimensionless distance of first realization of acceleration magnification M, for varying loading mach number m, using (4.27). Curves for X_M quickly converge to that of the shock location ($M \to \infty$) at higher values of M.

4.3 Ogden model

Another popular hyperelastic energy function commonly used to model incompressible soft solids is the Ogden model which is a multiparameter model expressed in terms of the principal stretches λ_i, which are the square root of eigenvalues of $\mathbf{B}$, and

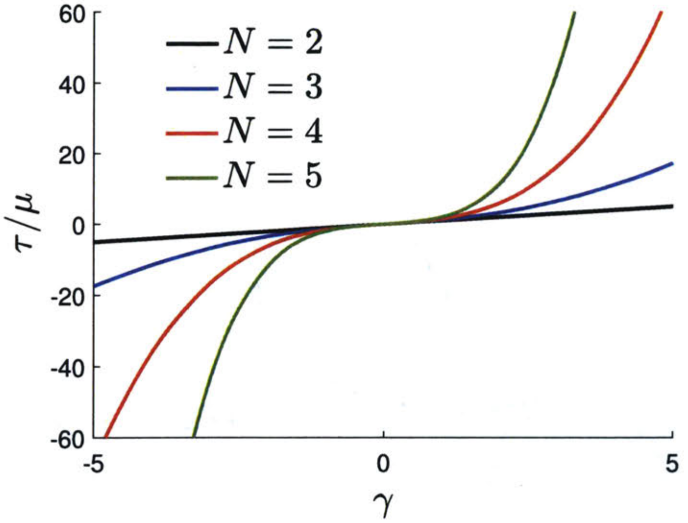

(a) Plot of the dimensionless shear stress as a function of the shear strain γ.

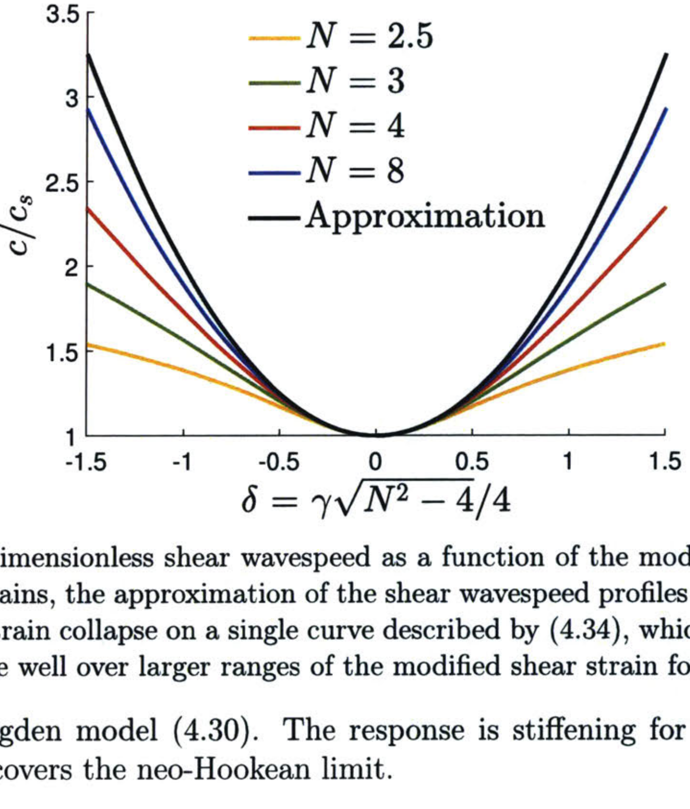

(b) Plot of the dimensionless shear wavespeed as a function of the modified shear strain δ. For moderate strains, the approximation of the shear wavespeed profiles as a function of the modified shear strain collapse on a single curve described by (4.34), which approximates the material response well over larger ranges of the modified shear strain for higher N.

Figure 4-11: Ogden model (4.30). The response is stiffening for $N > 2$ while the value $N = 2$ recovers the neo-Hookean limit.

material constants μ_p and N_p where $p = 1, 2, 3..., P$. For an incompressible material $\lambda_3 = 1/(\lambda_1\lambda_2)$ and we have the strain energy density function (Ogden, 1972),

$$W(\lambda_1, \lambda_2) = \sum_{p=1}^{P} \frac{2\mu_p}{N_p^2}\left(\lambda_1^{N_p} + \lambda_2^{N_p} + \lambda_1^{-N_p}\lambda_2^{-N_p} - 3\right) \tag{4.28}$$

where the linear elastic shear modulus is given by

$$\mu = \frac{1}{2}\sum_{p=1}^{N} \mu_p N_p \tag{4.29}$$

The Ogden model allows for a large number of parameters that can be chosen to fit different experimental stress-strain curves. Here we use the two parameter Ogden strain energy function for our analysis, i.e $P = 1$, such that $N = N_1$ and $\mu = \mu_1 N/2$ are the two independent material parameters that qualify the stress response of the material. The nonlinearity of the shear response is captured by the stiffening parameter N and the shear response is given by (using (4.28) in (2.7))

$$\tau(\gamma) = \frac{2\mu}{N}\frac{(\lambda_1^N - \lambda_1^{-N})}{\sqrt{4+\gamma^2}} \quad \text{where} \quad \lambda_1 = \frac{\gamma + \sqrt{\gamma^2+4}}{2} \tag{4.30}$$

The sign of N makes no difference to the shear stress response and hence we consider $N > 0$ here without loss of generality. Plots of the shear stress as a function of the shear strain are shown in Fig. 4-11(a), for different values of the material parameter N. The value of $N = 2$ yields the neo-Hookean shear response. We restrict our attention to materials with $N > 2$ for which the response is stiffening. The shear wavespeed for (4.30) can be found using (2.11), as

$$c(\gamma) = c_s\sqrt{\frac{2}{4+\gamma^2}\left(\lambda_1^N + \lambda_1^{-N} - \frac{\gamma\tau(\gamma)}{2\mu}\right)} \tag{4.31}$$

The large deformation Ogden model is not amenable to find closed form solutions using our analysis as the integration of $c(\gamma)$ is not analytically tractable (to find $Q(\gamma)$). With the goal of demonstrating similarity of results to the other stress models we make the assumption of moderate strains (such that $\gamma^2 >> \gamma^4$). This allows us to use series expansions about $\gamma = 0$, allowing for closed form expressions with the caveat of loss of accuracy at larger shear strains. Accordingly, the wavespeed (4.31) and its derivative can be expanded about $\gamma = 0$ as

$$c(\gamma) \approx c_s\left(1 + \frac{N^2-4}{16}\gamma^2\right) \quad , \quad \frac{\mathrm{d}c}{\mathrm{d}\gamma} \approx c_s\left(\frac{N^2-4}{8}\right)\gamma \tag{4.32}$$

Once again we assume $V \geq 0, \gamma \leq 0$ and from (3.32) we have $p_0 = 1, c_0 = c_s(N^2 - 4)/8$ for (4.32). Therefore the critical loading exponent n_c from (3.34) is once again 0.5, similar to the Gent model. Thus for loading exponents below 0.5, shocks are immediately formed for the stiffening Ogden solid (this result does not require the assumption of small/moderate strains). Further, $Q(\gamma)$ can be approximated as

$$Q(\gamma) \approx c_s\gamma\left(1 + \frac{(N^2-4)}{48}\gamma^2\right) \tag{4.33}$$

We define a modified strain $\delta = \gamma\sqrt{N^2-4}/4$, and functions of δ once again have a tilde accent. Functions of the shear strain $f(\gamma)$ can be written as $\tilde{f}(\delta) = f(4\delta/\sqrt{N^2-4})$ and thus the wavespeed from (4.32) becomes

$$\tilde{c}(\delta) \approx c_s(1+\delta^2) \tag{4.34}$$

Plots of the wavespeed as a function of the modified strain for different material stiffening parameters $N > 2$ are shown in Fig. 4-11(b), at moderate values of δ all the curves match well with the approximation (4.34). It can be seen that the more the stiffening (larger N), the larger the range of modified strain δ over which the approximation for wavespeed (4.34) is good[4].

We can use (4.18) and (4.21) for the Ogden solid as well, except that δ is now the modified strain and $\tilde{Q}$ is given by

$$\tilde{Q} = V_*\left(\delta + \frac{\delta^3}{3}\right) \quad \text{where} \quad V_* = \frac{4c_s}{\sqrt{N^2-4}} \tag{4.35}$$

Equation (4.18) once again provides a mapping $\hat{F}(\alpha) = \tilde{F}(\hat{\delta}(\alpha))$. We can divide

---

[4] At higher N larger range of δ still corresponds to low/moderate shear strains.

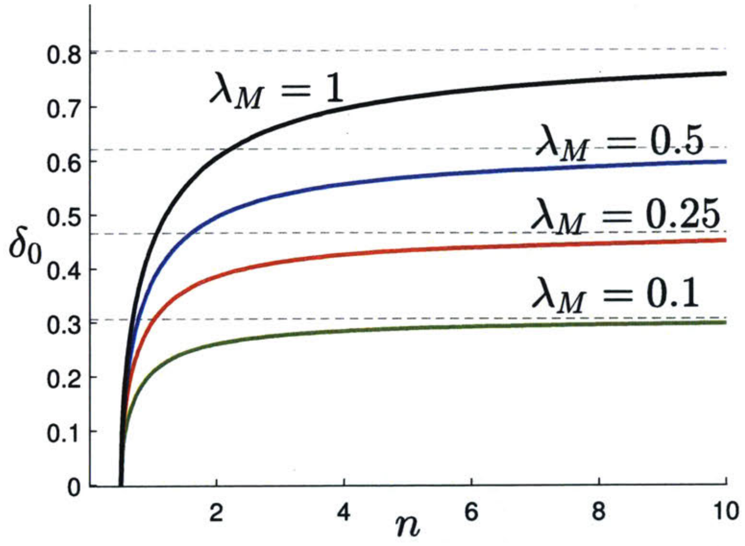

(a) Plots of δ_0, the positive root of (4.38), versus the loading exponent for different values of λ_M. The dotted lines represent the asymptotic value of δ_0 as $n \to \infty$ and $\delta_0 \to 0$ as $n \to 0.5$ (n_c).

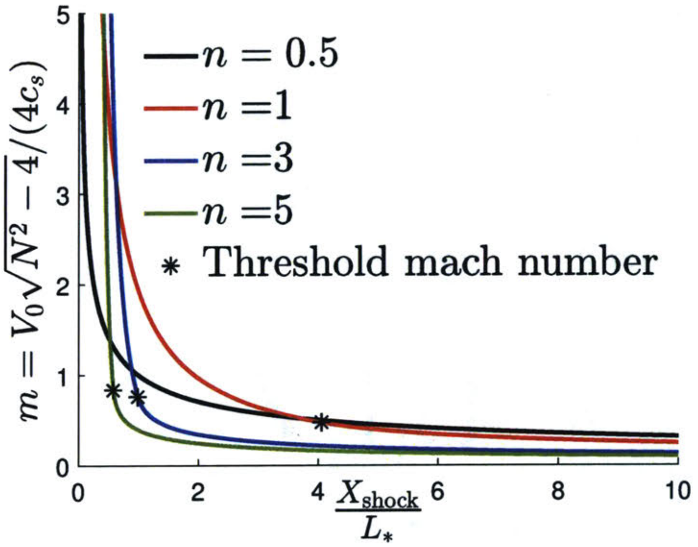

(b) Non-dimensional map of the shock location as a function of the loading mach number m, for various loading exponents (using $\lambda_M = 1$ in (4.40)). For $n > 0.5(n_c)$, a threshold mach number (m_{th}) separates two different functional forms of X_{shock}/L_*. In different loading mach number regimes different loading exponents might delay shock formation.

Figure 4-12: Ogden model (4.30) for $N > 2$.

(4.18) and (4.35) by V_* to write

$$\tilde{q}(\delta) = \frac{Q(\delta)}{V_*} = -\frac{V}{V_*} \quad \Rightarrow \quad \delta = -\tilde{q}^{-1}\left(\frac{V}{V_*}\right) \quad \text{where} \quad \tilde{q}(\delta) = \delta + \frac{\delta^3}{3} \tag{4.36}$$

and $|\tilde{q}(\delta)|$ is once again the local mach number, different from the loading mach number m. We can specialize (4.21) for the Ogden solid as (see Appendix A.3.3)

$$X_M = \frac{L_*\lambda_M}{n m^{\frac{1}{n}}} \frac{K_{\text{og}}(\delta)}{\left(-q(\delta)\right)^{\frac{n-1}{n}}} \quad , \quad K_{\text{og}}(\delta) = \frac{-\,(1+\delta^2)^3}{2\delta} \tag{4.37}$$

where m and L_* are defined in (4.9).

Evaluating all the different functions in terms of δ and substituting them in (3.36) we end up with (see Appendix A.3.3)

$$\frac{\mathrm{d}t^\alpha_M}{\mathrm{d}\alpha} = \tilde{G}(\delta) = 1 + \frac{3\lambda_M}{2} - \frac{\lambda_M}{2\delta^2} - \frac{3(1+\delta^2)^2}{2\delta^2(3+\delta^2)} \frac{(n-1)\lambda_M}{n} \tag{4.38}$$

For $n = 0.5$, once again we can verify that $\frac{\mathrm{d}t^\alpha_M}{\mathrm{d}\alpha} = \tilde{G}$ is positive for all δ and thus, $\alpha^M_{\text{min}} = \delta^M_{\text{min}} = 0$. Hence, acceleration magnification and shock formation initiates at the leading edge of the waveform form for $n = n_c$, as before. For $n = 0.5(n_c)$, we have using (3.21) and (3.35)[2]

$$X_M = X^\alpha_M \Big|_{\alpha^M_{\text{min}}} = X^0_M \Big|_{n=n_c} = \frac{16 c_s^3\, t_0 \lambda_M}{(N^2-4)V_0^2} = \frac{L_*\lambda_M}{m^2} \tag{4.39}$$

For $n > 0.5$ the plot of $\frac{\mathrm{d}t^\alpha_M}{\mathrm{d}\alpha}$ vs $|\delta|$ resembles that in Fig. 4-7(a), with a zero, $\delta_0 \in (0,1)$. The discussion of δ_0 for the Gent solid holds for the Ogden solid as well except δ here refers to the modified strain instead of the fractional shear strain and Fig. 4-12(a) shows the plots of δ_0 for an Ogden solid. Similarly (4.26) also applies for the Gent solid where $\tilde{q}$ is now given by (4.36). Plugging (4.26) into (4.37), and using the result (4.39) we obtain the solution for non dimensionalised X_M at moderate strains for stiffening ($N > 2$) Ogden solids (see Appendix A.3.3),

$$\frac{X^M}{L^*} = \lambda_M \begin{cases} 0 & n < 0.5,\ m \geq 0 \\ \dfrac{1}{m^2} & n = 0.5,\ m \geq 0 \\ \dfrac{K_{\text{og}}(-\delta_0(\lambda_M, n))}{n\ m^{\frac{1}{n}}\ m_{\text{th}}^{\frac{n-1}{n}}} & n > 0.5,\ m \geq m_{\text{th}} \\ \dfrac{K_{\text{og}}\big|_{-\tilde{q}^{-1}(m)}}{n\ m} & n > 0.5,\ 0 \leq m < m_{\text{th}} \end{cases} \tag{4.40}$$

Here $m_{\text{th}} = \tilde{q}(\delta_0(\lambda_M, n))$ and $\delta_0(\lambda_M, n)$ is the positive root of $\tilde{G}(\delta)$ in (4.38). Setting $\lambda_M = 1$ gives the expressions for X_{shock}/L^* for the incompressible stiffening Ogden solid. Once again it can be verified that the only discontinuity in the solution space is in moving from $n \to {n_c}^-$ to n_c (0.5 for Ogden solid). The results for a stiffening Ogden solid (at moderate strains) are shown in Fig. 4-12(b) and Figs. 4-13-4-14, and are similar in nature to the results for the Gent model. A larger N corresponds to higher material nonlinearity similar to a larger k in the exponential stress model and smaller J_m in the Gent model. All the observations made for the results of the Gent model also hold for the stiffening Ogden model when the strains are moderate ($\gamma^2 >> \gamma^4$). The general nature of results might hold for large strains as well though closed form solutions were not attainable here.

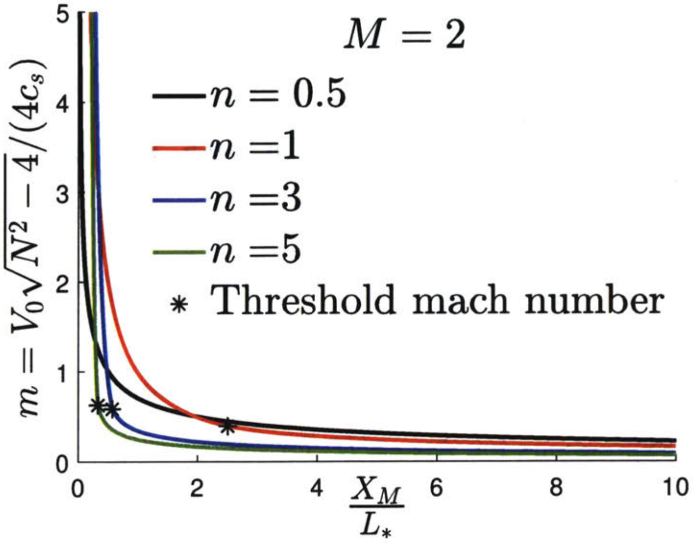

(a)

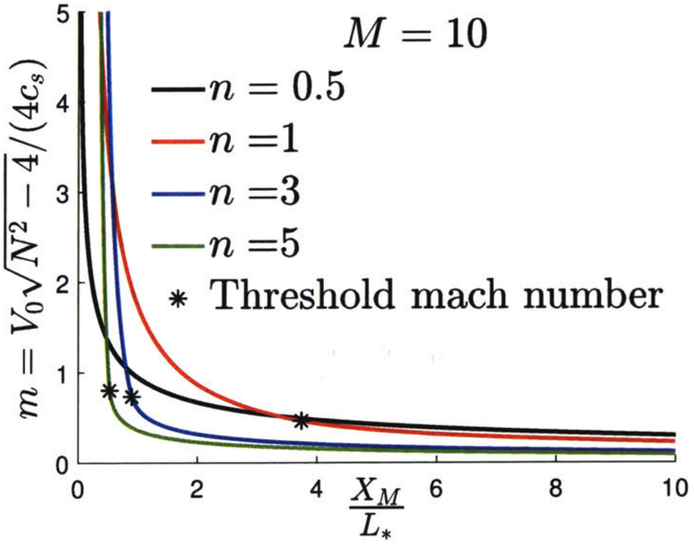

(b)

Figure 4-13: Ogden model (4.30) for $N > 2$: Maps of the dimensionless distance of first realization of acceleration magnification M, for varying loading mach number m and different loading exponents n, using (4.40).

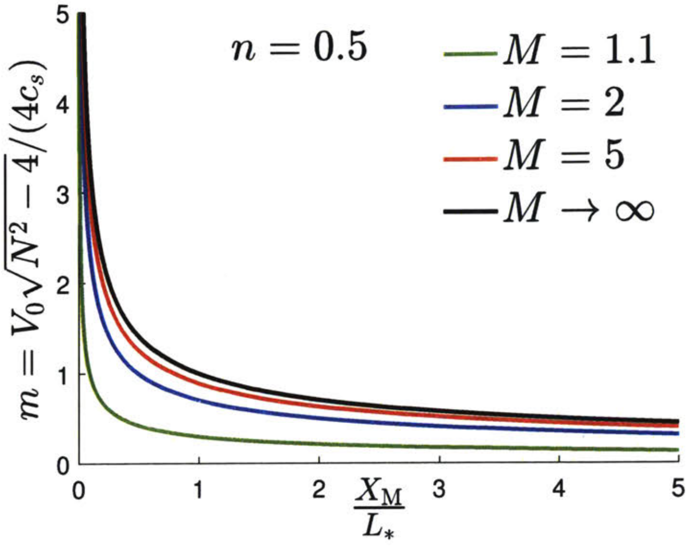

(a) Maps at different M for $n = 0.5(n_c)$.

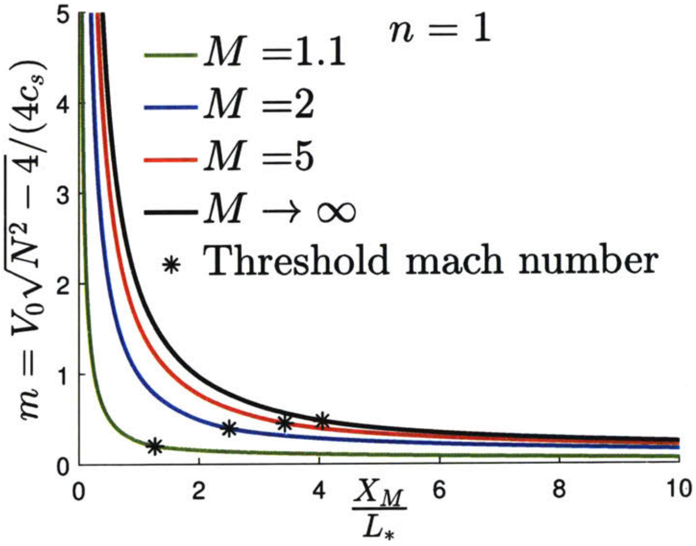

(b) Maps at different M for $n = 1$.

Figure 4-14: Ogden model (4.30) for $N > 2$: Maps of the dimensionless distance of first realization of acceleration magnification M, for varying loading mach number m, using (4.40). Curves for X_M quickly converge to that of the shock location ($M \to \infty$) at higher values of M.

Chapter 5

Example application to shear shock formation in brain tissue

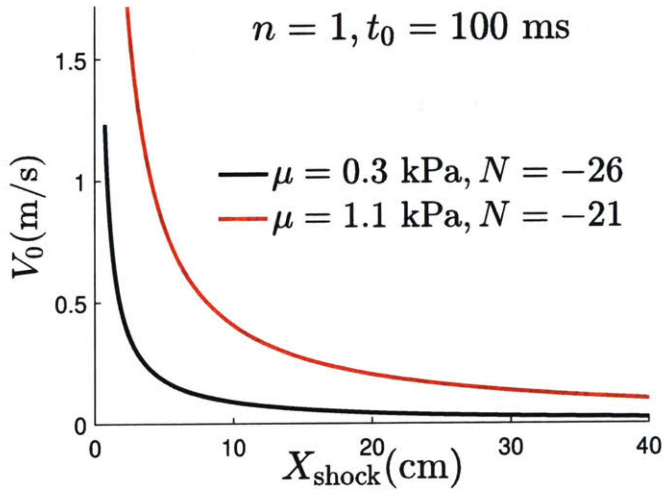

Figure 5-1: Shock formation in the brain: Plot of the shock formation distance for the two parameter Ogden model (4.30), as a function of the ramp shear velocity V_0, for a linear ramping ($n = 1$ in the loading (3.28)) and ramp time of 100 ms, using (4.40). The two curves shown are the maximum and minimum shock formation distances for the range of Ogden parameter values reported in Budday et al. (2017) for simple shear loading of the human brain. For the range of V_0 shown, the magnitude of shear strains generated is below 0.5.

Having quantified shear shock evolution for different hyperelastic models in the previous chapter, we now apply our results to a physical problem of interest. Recently, Espíndola et al. (2017) demonstrated the evolution of smooth shear waves into shear shocks in a porcine brain, showing an acceleration amplification factor of up to $M \approx 8.5$ at the shock front; the magnification is not infinite as in our study, since the brain tissue has some viscosity. Nonetheless, it was seen in the previous chapter that high magnifications of that order are attained practically close to the shock location. In Espíndola et al. (2017), it was suggested that shear shock waves could be a previously unappreciated mechanism that could play a significant role in traumatic brain injuries (TBI). To investigate shear shock formation in the brain using our results, we idealize the brain as an isotropic hyperleastic body and neglect boundary effects and reflections. We also ignore viscosity and any spatial variation in properties. The Ogden model is the most commonly used hyperelastic model for constitutive studies of the brain and consequently we will use our results for the two parameter Ogden model.

The mechanical response of the human brain was carefully and systematically studied across different brain regions for various loading modes in Budday et al. (2017) and it was demonstrated that popular hyperelastic models are unable to accurately capture the stress response across different loading modes with a single set of parameters. However, we are primarily interested in the shear response of the brain and we make use of the parameters reported for the simple shear testing. For the two parameter Ogden shear response (4.30), averaged parameter values for μ in the range of $0.3 - 1.1$ kPa and for N in the range of -26 to -21 were reported for different regions of the brain. We take the density of the brain to be $\rho_0 = 1000$ kg/m^3 which yields c_s in the range of $0.5 - 1.1$ m/s. Assuming that a shear impact of the brain can be represented by the loading (3.28), we consider a linear ramping ($n = 1$) from zero velocity to an impact velocity V_0, over an impact time of $t_0 = 100$ ms. Using these loading and material parameters in (4.40), we can make a plot of the shock formation distance as a function of the impact velocity as shown in Fig. 5-1. The two curves shown are for the material parameter values, from the range of reported values, that predict minimum and maximum shock distance. Thus, for a given impact we have a range of distances within which a shock is expected to form for an arbitrary brain sample. As discussed in the previous chapter, a brain that has a lower μ and higher nonlinearity parameter (N), evolves a shock over a shorter distance for a given impact. Since the Ogden parameter values were reported for tests conducted in the strain magnitude range of $0 - 0.2$ and since our results for the Ogden solid are more accurate for moderate strains we cap the curves at impact velocity values that would generate a shear strain of[1] 0.5. Shock formation distance for any impact time can be obtained by remembering that the shock formation distance scales linearly with t_0.

We can readily use Fig. 5-1 in a design problem such as that of a helmet to avoid shear shocks in the brain. Since the average length of the human brain is 15 cm, from Fig. 5-1, we find a conservative[2] maximum velocity of $\sim$ 6 cm/s that can be safely transferred to the brain after dissipation by the helmet and the skull, to avoid shear shocks. Also, the order of shock distances predicted by our analysis for the brain tissue is in agreement with the experimental values in Espíndola et al. (2017) where shocks (peak acceleration magnification) occur at distances of the order of 1 cm for shear velocities of the order 1 m/s and time periods of the order 100 ms. These results also suggest that experiments conducted on small brain samples in TBI research might not be able to capture shear shocks that could evolve in a real brain subjected to the same loading. Nevertheless, the non-dimensional maps can be used to rescale the loading waveform so that similar features of the shock evolution can be observed at smaller scales. Finally, it can be clearly seen that larger brains are more susceptible to shear shocks.

---

[1] Maximum value of $V_0 = Q(\gamma = 0.5)$.

[2] Viscosity would allow for higher impact velocities without shock formation.

Chapter 6

Concluding Remarks & Future Work

6.1 Conclusions

The nonlinear evolution of a loading shear wave into a shear shock was studied for incompressible strain stiffening hyperelastic solids using the method of characteristics in the framework of large deformation elastodynamics. A general family of loading waveforms was considered and closed form solutions for the distance of first shock formation or realization of a given acceleration magnification were obtained for three different stress models. The results were encapsulated in non-dimensional maps, formulated in terms of a loading mach number and the loading exponent. The maps can guide design selection of loading, and material parameters and dimensions, to avoid shock formation. The singularity of the loading required to immediately form shocks was quantified through a critical loading exponent. For weaker loadings a critical mach number, dependent on the loading waveform shape exists above and below which the functional forms of the evolution distances are different. Larger loadings over shorter times and/or higher material nonlinearity lead to shock evolution over shorter distances. The dependence of the shock evolution on the load profile shape was shown to be non-trivial and different shapes were seen to be better at delaying shock formation depending on the loading mach regime. We hope that our non-dimensional maps can guide design of protective structures and also that this work will serve as a stepping stone for future studies of nonlinear wave evolution in solids in the large deformation elastodynamics framework.

6.2 Future Work

Future directions include extension to coupled longitudinal and shear waves in compressible solids, inclusion of viscosity, and studying the evolution post shock initiation (see Appendix B). Also of interest would be the inclusion of anisotropy, heterogeneity, and boundary effects in the analysis, as they might become relevant for shear shock evolution in biological systems.

Appendix A

Solution for loading (3.28)

A.1 Derivation of X_M, t^0_M

We have from (3.27),

$$t^0_M = -\, c_s^2 \lim_{\substack{\alpha \to 0^+ \\ \gamma \to 0^-}} \left(V'(\alpha) \frac{\mathrm{d}c}{\mathrm{d}\gamma} \right)^{-1} \tag{A.1}$$

For the loading (3.28), using (3.2b)

$$Q(\gamma) = -V_0 \left(\frac{\alpha}{t_0} \right)^n \quad , \quad \alpha \le t_0 \tag{A.2}$$

Thus

$$V'(\alpha) = \frac{nV_0}{t_0} \left(\frac{\alpha}{t_0} \right)^{n-1} = \frac{nV_0}{t_0} \left(\frac{-Q(\gamma)}{V_0} \right)^{\frac{n-1}{n}} \quad , \quad \alpha < t_0 \tag{A.3}$$

Substituting (A.3) in (3.22b), we obtain

$$X_M = \lambda_M \left. \frac{\psi c}{\frac{nV_0}{t_0} \left(\frac{-Q(\gamma)}{V_0} \right)^{\frac{n-1}{n}}} \right|_{\gamma^M_{\text{min}}} = \frac{t_0 \lambda_M}{n V_0^{\frac{1}{n}}} \left. \frac{\psi c}{(-Q(\gamma))^{\frac{n-1}{n}}} \right|_{\gamma^M_{\text{min}}} \quad , \quad \gamma^M_{\text{min}} = \hat{\gamma}(\alpha^M_{\text{min}}) \tag{A.4}$$

Substituting (A.3) in (A.1) and using $Q(\gamma) \to c_s \gamma$ as $\gamma \to 0$, we can write (we assume $V \ge 0, \gamma \le 0$),

$$t^0_M = \frac{c_s^{1+\frac{1}{n}}\, t_0 \lambda_M}{n V_0^{1/n}} \lim_{\gamma \to 0^-} - \left(\frac{\mathrm{d}c}{\mathrm{d}\gamma} \right)^{-1} (-\gamma)^{\frac{1-n}{n}} \tag{A.5}$$

A.2 Derivation of $\frac{\mathrm{d}t_M^\alpha}{\mathrm{d}\alpha}$

We have from (3.22a)

$$t_M^\alpha = \alpha + \lambda_M \frac{\hat{\psi}}{V'(\alpha)} \tag{A.6}$$

Thus

$$\frac{\mathrm{d}t_M^\alpha}{\mathrm{d}\alpha} = 1 + \frac{\hat{\psi}'}{V'(\alpha)}\lambda_M - \frac{\hat{\psi}V''(\alpha)\lambda_M}{(V'(\alpha))^2} \tag{A.7}$$

For $\alpha \in [0, t_0]$ and the loading (3.28), using (3.2b) we can write

$$\frac{V''(\alpha)}{(V'(\alpha))^2} = \frac{n-1}{nV(\alpha)} = -\frac{n-1}{n\hat{Q}} \quad , \quad \alpha \in [0, t_0] \tag{A.8}$$

We also have using (3.7),

$$\frac{\hat{\psi}'}{V'(\alpha)} = \frac{\frac{\mathrm{d}\psi}{\mathrm{d}\gamma}\hat{\gamma}'}{V'(\alpha)} = -\frac{\mathrm{d}\psi}{\mathrm{d}\gamma}c^{-1} \tag{A.9}$$

Thus the derivative $\frac{\mathrm{d}t_M^\alpha}{\mathrm{d}\alpha}$ for $\alpha \in [0, t_0]$ is ,

$$\Rightarrow \frac{\mathrm{d}t_M^\alpha}{\mathrm{d}\alpha} = \hat{G}(\alpha) = 1 + \hat{R}\lambda_M + \frac{\hat{\psi}(n-1)\lambda_M}{\hat{Q}n} \quad , \quad R(\gamma) = -\frac{\mathrm{d}\psi}{\mathrm{d}\gamma}c^{-1} \tag{A.10}$$

Using $\psi(\gamma) = -c^2\left(\frac{\mathrm{d}c}{\mathrm{d}\gamma}\right)^{-1}$, we have $R(\gamma) = -\frac{\mathrm{d}\psi}{\mathrm{d}\gamma}c^{-1} = 2 - c\frac{\mathrm{d}^2c}{\mathrm{d}\gamma^2}\left(\frac{\mathrm{d}c}{\mathrm{d}\gamma}\right)^{-2}$ and thus

$$G(\gamma) = 1 + 2\lambda_M - \frac{c\lambda_M}{(\frac{\mathrm{d}c}{\mathrm{d}\gamma})^2}\frac{\mathrm{d}^2c}{\mathrm{d}\gamma^2} - \frac{(n-1)\lambda_M}{n}\frac{c^2}{Q\frac{\mathrm{d}c}{\mathrm{d}\gamma}} \tag{A.11}$$

A.3 Application to material models

A.3.1 Exponential model

In this section $\gamma < 0$,

$$c(\gamma) = c_s e^{-\frac{k}{2}\gamma} \quad , \quad \frac{\mathrm{d}c}{\mathrm{d}\gamma} = -\frac{c_s k}{2}e^{-k\frac{\gamma}{2}} \quad , \quad \psi(\gamma) = V_* e^{-k\frac{\gamma}{2}} \quad , \quad R(\gamma) = -\frac{\mathrm{d}\psi}{\mathrm{d}\gamma}c^{-1} = 1 \tag{A.12}$$

From (4.5) we have $e^{-\frac{k}{2}\gamma} = 1 + V/V_*$, which along with (A.12) yields (4.6).

Evaluation of α^M_{min} for $n > 1$: Differentiating (4.7) we have

$$\frac{\mathrm{d}^2 t^\alpha_M}{\mathrm{d}\alpha^2} = \frac{(n-1)\lambda_M}{nV^2} V'(\alpha) \tag{A.13}$$

Substituting the loading (3.28) for $\alpha \le t_0$ in (A.13) we obtain

$$\frac{\mathrm{d}^2 t^\alpha_M}{\mathrm{d}\alpha^2} = \frac{(n-1)\lambda_M V_*}{\alpha V} \tag{A.14}$$

Thus $\frac{\mathrm{d}^2 t^\alpha_M}{\mathrm{d}\alpha^2} > 0$ for $n > 1$ and $\alpha \le t_0$, and thus we can find α^M_{min} using (4.7) and (3.28) as

$$\left.\frac{\mathrm{d}t^\alpha_M}{\mathrm{d}\alpha}\right|_{\alpha^M_{\text{min}}} = 0 \quad \Rightarrow \quad \frac{V(\alpha^M_{\text{min}})}{V_*} = m\left(\frac{\alpha^M_{\text{min}}}{t_0}\right)^n = \frac{(n-1)\lambda_M}{n+\lambda_M} = m_{\text{th}} \quad , \quad \alpha^M_{\text{min}} \in [0, t_0] \tag{A.15}$$

Equation (A.15) has a solution $\alpha^M_{\text{min}} \in [0, t_0]$ for $n > 1$ only if the loading mach number m is greater than or equal to m_{th}. For $m < m_{\text{th}}$, $\alpha^M_{\text{min}} = t_0$ since $\frac{\mathrm{d}t^\alpha_M}{\mathrm{d}\alpha} < 0$ for $\alpha \in [0, t_0]$ (Using $V/V_* < m < m_{\text{th}}$ in (4.7)). Using (A.15), for $m \ge m_{\text{th}}$,

$$\alpha^M_{\text{min}} = t_0\left(\frac{m_{\text{th}}}{m}\right)^{\frac{1}{n}} \tag{A.16}$$

Evaluation of X_M/L_* for $n > 1$: Substituting (4.6) and the loading (3.28) for $t < t_0$ in (3.22b) we obtain

$$X_M = c_s t_0^n \lambda_M \; \frac{(V(\alpha^M_{\text{min}}) + V_*)\big(1 + \frac{V(\alpha_{\text{min}})}{V_*}\big)}{nV_0(\alpha^M_{\text{min}})^{n-1}} = c_s t_0^n \lambda_M \; \frac{(\frac{V(\alpha^M_{\text{min}})}{V_0} + \frac{1}{m})\big(1 + \frac{V(\alpha^M_{\text{min}})}{V_*}\big)}{n(\alpha^M_{\text{min}})^{n-1}} \tag{A.17}$$

From (4.10) and (3.28), for $n > 1$ and $m < m_{\text{th}}$, we have $\alpha^M_{\text{min}} = t_0, V(\alpha^M_{\text{min}}) = V_0$, and thus (A.17) becomes

$$X_M = \frac{c_s t_0 \lambda_M}{n}\left(1+\frac{1}{m}\right)(1+m) \Rightarrow \frac{X_M}{L_*} = \frac{\lambda_M}{n}\left(2+m+\frac{1}{m}\right) \quad \text{for } n>1, m<m_{\text{th}} \tag{A.18}$$

From (4.10) and (3.28), for $n > 1$ and $m \geq m_{\text{th}}$ we have $\alpha^M_{\text{min}} = t_0\left(\frac{m_{\text{th}}}{m}\right)^{\frac{1}{n}}$, $V(\alpha^M_{\text{min}})/V_0 = m_{\text{th}}/m$, and thus (A.17) becomes

$$X_M = L_*\lambda_M \frac{(1+m_{\text{th}})^2\left(\frac{m_{\text{th}}}{m}\right)^{\frac{1}{n}}}{n\, m_{\text{th}}} \Rightarrow \frac{X_M}{L_*} = \frac{n(1+\lambda_M)^2}{(n-1)(n+\lambda_M)}\left(\frac{m_{\text{th}}}{m}\right)^{\frac{1}{n}} \quad \text{for } n>1, m\geq m_{\text{th}} \tag{A.19}$$

where we have used $m_{\text{th}} = \frac{(n-1)\lambda_M}{n+\lambda_M}$.

Solution continuity: We demonstrate the continuity of the solution (4.12) at $n \to 1^+$ and $m \to m_{\text{th}}^-$. We have $m_{\text{th}} = \frac{(n-1)\lambda_M}{n+\lambda_M}$ and thus for $n \to 1$, $m_{\text{th}} \to 0$. This means that only the $m \geq m_{\text{th}}$ case for $n > 1$ is relevant for $n \to 1^+$ in (4.12). Setting $n \to 1^+$ for that case recovers the $n = 1$ case,

$$\frac{X_M}{L_*} = \lim_{n\to 1^+} \frac{n(1+\lambda_M)^2}{(n-1)(n+\lambda_M)}\left(\frac{(n-1)\lambda_M}{(n+\lambda_M)m}\right)^{\frac{1}{n}} = \frac{\lambda_M}{m} \tag{A.20}$$

Setting $m = m_{\text{th}}$ in the $n \geq 1, m \geq m_{\text{th}}$ case in (4.12) yields

$$\frac{X_M}{L_*} = \frac{n(1+\lambda_M)^2}{(n-1)(n+\lambda_M)} \tag{A.21}$$

Setting $m \to m_{\text{th}}^-$ in the $n \geq 1, m < m_{\text{th}}$ case in (4.12) recovers (A.21),

$$\frac{X_M}{L_*} = \frac{\lambda_M}{n}\left(\frac{(m_{\text{th}}+1)^2}{m_{\text{th}}}\right) = \frac{n(1+\lambda_M)^2}{(n-1)(n+\lambda_M)} \tag{A.22}$$

Shortest distance of realization of acceleration magnification: Let us denote the shortest distance from the loading surface at which a given magnification M is realized by X^s_M. For $n < n_c$, X_M and X^s_M are both zero. For $n > n_c, m < m_{\text{th}}$, the derivative $\frac{\mathrm{d}t^\alpha_M}{\mathrm{d}\alpha}$ is always negative in the ramping interval (Using $V/V_* < m < m_{\text{th}}$ in (4.7)) and thus using (3.23), $\frac{\mathrm{d}X^\alpha_M}{\mathrm{d}\alpha}$ is also negative during ramping. Thus the characteristic $\alpha = t_0$ will minimize both t^α_M and X^α_M and hence once again X_M and X^s_M are equal. For $n = n_c$, the derivative $\frac{\mathrm{d}t^\alpha_M}{\mathrm{d}\alpha}$ is always positive and greater than one (from (4.7)) and hence, using (3.23) $\frac{\mathrm{d}X^\alpha_M}{\mathrm{d}\alpha}$ is also always positive. Thus the characteristic $\alpha = 0$ will minimize both t^α_M and X^α_M, and thus X_M and X^s_M are equal once more. For the case $n > n_c, m > m_{\text{th}}$, the distances X_M and X^s_M will not be the same. The same observations made here can be verified for the Gent and Ogden models as well where n_c will be 0.5 for them.

A.3.2 Gent model

Evaluating the different expressions for the Gent solid,

$$c(\gamma) = \sqrt{\frac{1}{\rho_0}\frac{\partial \tau}{\partial \gamma}} = V_* \frac{\sqrt{J_m + \gamma^2}}{J_m - \gamma^2} \quad , \quad \tilde{c}(\delta) = c_s \frac{\sqrt{1+\delta^2}}{1-\delta^2} \tag{A.23}$$

$$\begin{aligned} Q(\gamma) &= V_* \left(\sqrt{2} \tanh^{-1} \left(\frac{\sqrt{2}\gamma}{\sqrt{J_m + \gamma^2}} \right) - \log \left(\frac{\gamma + \sqrt{J_m + \gamma^2}}{\sqrt{J_m}} \right) \right) \\ &= V_* \log \left(\frac{\left(\frac{\sqrt{J_m+\gamma^2}+\gamma\sqrt{2}}{\sqrt{J_m+\gamma^2}-\gamma\sqrt{2}} \right)^{\frac{1}{\sqrt{2}}}}{\frac{\gamma+\sqrt{J_m+\gamma^2}}{\sqrt{J_m}}} \right) \qquad \text{As } \gamma \to 0, \quad \mathrm{Q}(\gamma) \to \mathrm{c_s}\gamma \end{aligned} \tag{A.24}$$

$$\tilde{Q}(\delta) = V_* \log \left(\frac{\left(\frac{\sqrt{1+\delta^2}+\delta\sqrt{2}}{\sqrt{1+\delta^2}-\delta\sqrt{2}} \right)^{\frac{1}{\sqrt{2}}}}{\delta + \sqrt{1+\delta^2}} \right) \qquad \text{As } \delta \to 0, \quad \tilde{\mathrm{Q}}(\delta) \to \mathrm{c_s}\sqrt{\mathrm{J_m}}\delta \tag{A.25}$$

$$\tilde{q}(\delta) = \frac{Q(\delta)}{V^*} = \log \left(\frac{\left(\frac{\sqrt{1+\delta^2}+\delta\sqrt{2}}{\sqrt{1+\delta^2}-\delta\sqrt{2}} \right)^{\frac{1}{\sqrt{2}}}}{\delta + \sqrt{1+\delta^2}} \right) \tag{A.26}$$

$$\frac{\mathrm{d}c(\gamma)}{\mathrm{d}\gamma} = f_1(\gamma) = \frac{c_s\sqrt{J_m}\gamma(3J_m + \gamma^2)}{(J_m - \gamma^2)^2\sqrt{J_m + \gamma^2}} \quad , \quad \tilde{f}_1(\delta) = \frac{c_s\delta(3+\delta^2)}{\sqrt{J_m}(1-\delta^2)^2\sqrt{1+\delta^2}} \tag{A.27}$$

$$\psi(\gamma) = -\frac{c^2(\gamma)}{f_1(\gamma)} = -\frac{V_*(J_m + \gamma^2)^{\frac{3}{2}}}{\gamma(3J_m + \gamma^2)} \quad , \quad \tilde{\psi}(\delta) = -\frac{V_*(1+\delta^2)^{\frac{3}{2}}}{\delta(3+\delta^2)} \tag{A.28}$$

$$\frac{\mathrm{d}\psi(\gamma)}{\mathrm{d}\gamma} = -\frac{3c_s J_m^{\frac{3}{2}}(\gamma^2 - J_m)\sqrt{J_m + \gamma^2}}{\gamma^2(3J_m + \gamma^2)^2} \tag{A.29}$$

$$R(\gamma) = -\frac{\mathrm{d}\psi}{\mathrm{d}\gamma}c^{-1} = -\frac{3J_m(J_m - \gamma^2)^2}{\gamma^2(3J_m + \gamma^2)^2} \quad , \quad \tilde{R}(\delta) = \frac{-3(1-\delta^2)^2}{\delta^2(3+\delta^2)^2} \tag{A.30}$$

Substituting the above expressions in (3.36) and using (4.20) we obtain ($\tilde{G}(\delta) = \tilde{G}(\hat{\delta}(\alpha)) = \hat{G}(\alpha)$)

$$\frac{\mathrm{d}t_M^\alpha}{\mathrm{d}\alpha} = \tilde{G}(\delta) = 1 - \frac{3(1-\delta^2)^2\lambda_M}{\delta^2(3+\delta^2)^2} - \frac{(1+\delta^2)^{\frac{3}{2}}}{\delta(3+\delta^2)}\frac{(n-1)V_*\lambda_M}{n\tilde{Q}(\delta)} \tag{A.31}$$

$$= 1 - \frac{3(1-\delta^2)^2\lambda_M}{\delta^2(3+\delta^2)^2} - \frac{(1+\delta^2)^{\frac{3}{2}}}{\delta(3+\delta^2)}\frac{(n-1)\lambda_M}{n\tilde{q}(\delta)} \tag{A.32}$$

Using (A.23) and (A.28) in (4.21) we have

$$X_M = \frac{\lambda_M t_0}{nV_0^{\frac{1}{n}}}\left.\frac{\tilde{\psi}\tilde{c}}{(-\tilde{Q}(\delta))^{\frac{n-1}{n}}}\right|_{\delta^M_{\min}} = \frac{c_s t_0 V_* \lambda_M}{nV_0^{\frac{1}{n}}}\left.\frac{-(1+\delta^2)^2}{\delta(3+\delta^2)(1-\delta^2)(-Q(\delta))^{\frac{n-1}{n}}}\right|_{\delta^M_{\min}} \tag{A.33}$$

$$= \frac{c_s t_0 V_*^{\frac{1}{n}}\lambda_M}{nV_0^{\frac{1}{n}}}\left.\frac{K(\delta)}{(-q(\delta))^{\frac{n-1}{n}}}\right|_{\delta^M_{\min}} = \frac{L_*\lambda_M}{nm^{\frac{1}{n}}}\left.\frac{K(\delta)}{(-q(\delta))^{\frac{n-1}{n}}}\right|_{\delta^M_{\min}} \tag{A.34}$$

Using (4.26) in (A.34) we obtain

$$\frac{X^M}{L^*} = \frac{\lambda_M}{nm^{\frac{1}{n}}}\begin{cases} \dfrac{K(-\delta_0(\lambda_M, n))}{m_{\text{th}}^{\frac{n-1}{n}}} & m \geq m_{\text{th}}, n > 0.5 \\ \dfrac{K\big|_{-\tilde{q}^{-1}(m)}}{m^{\frac{n-1}{n}}} & m < m_{\text{th}}, n > 0.5 \end{cases} \tag{A.35}$$

A.3.3 Ogden model

Under the assumptions of moderate strains, for the Ogden model we have

$$c(\gamma) \approx c_s\left(1 + \frac{N^2-4}{16}\gamma^2\right) \quad , \quad \tilde{c} \approx c_s(1+\delta^2) \quad , \quad \delta = \frac{\sqrt{N^2-4}}{4}\gamma \tag{A.36}$$

$$Q(\gamma) \approx c_s\gamma(1+\frac{N^2-4}{48}\gamma^3) \quad , \quad Q(\delta) = V_*\delta\left(1+\frac{\delta^2}{3}\right) \quad , \quad V_* = \frac{4c_s}{\sqrt{N^2-4}} \tag{A.37}$$

$$\tilde{q}(\delta) = \frac{Q(\delta)}{V^*} \approx \delta + \frac{\delta^3}{3} \tag{A.38}$$

$$\frac{\mathrm{d}c(\gamma)}{\mathrm{d}\gamma} = f_1(\gamma) \approx c_s\frac{N^2-4}{8}\gamma \quad , \quad \tilde{f}_1(\delta) = c_s\frac{\sqrt{N^2-4}}{2}\delta \quad , \quad \frac{\mathrm{d}^2c(\gamma)}{\mathrm{d}\gamma^2} \approx c_s\frac{N^2-4}{8} \tag{A.39}$$

$$\psi(\gamma) = -\frac{c^2(\gamma)}{f_1(\gamma)} \approx -\frac{8c_s(1+\frac{N^2-4}{16}\gamma^2)^2}{(N^2-4)\gamma} \quad , \quad \tilde{\psi}(\delta) = -\frac{V_*(1+\delta^2)^2}{2\delta} \tag{A.40}$$

Substituting the above expressions in (A.11) we obtain

$$\tilde{G}(\delta) = 1 + 2\lambda_M - \frac{\lambda_M(1+\delta^2)}{2\delta^2} - \frac{3(1+\delta^2)^2}{2\delta^2(3+\delta^2)}\frac{(n-1)\lambda_M}{n} \tag{A.41}$$

$$= 1 + \frac{3\lambda_M}{2} - \frac{\lambda_M}{2\delta^2} - \frac{3(1+\delta^2)^2}{2\delta^2(3+\delta^2)}\frac{(n-1)\lambda_M}{n} \tag{A.42}$$

Using (A.36) and (A.40) in (4.21) we have

$$X_M = \frac{\lambda_M t_0}{nV_0^{\frac{1}{n}}} \left.\frac{\tilde{\psi}\tilde{c}}{(-\tilde{Q}(\delta))^{\frac{n-1}{n}}}\right|_{\delta^M_{\min}} = \frac{c_s t_0 V_* \lambda_M}{nV_0^{\frac{1}{n}}} \left.\frac{-(1+\delta^2)^3}{2\delta(-Q(\delta))^{\frac{n-1}{n}}}\right|_{\delta^M_{\min}} \tag{A.43}$$

$$= \frac{c_s t_0 V_*^{\frac{1}{n}} \lambda_M}{nV_0^{\frac{1}{n}}} \left.\frac{K_{\mathrm{og}}(\delta)}{(-q(\delta))^{\frac{n-1}{n}}}\right|_{\delta^M_{\min}} = \frac{L_*\lambda_M}{nm^{\frac{1}{n}}} \left.\frac{K_{\mathrm{og}}(\delta)}{(-q(\delta))^{\frac{n-1}{n}}}\right|_{\delta^M_{\min}} \tag{A.44}$$

Plugging (4.26) in (A.44) we obtain

$$\frac{X^M}{L^*} = \frac{\lambda_M}{nm^{\frac{1}{n}}} \begin{cases} \dfrac{K_{\mathrm{og}}(-\delta_0(\lambda_M, n))}{m_{\mathrm{th}}^{\frac{n-1}{n}}} & m \geq m_{\mathrm{th}}, n > 0.5 \\ \dfrac{K_{\mathrm{og}}\big|_{-\tilde{q}^{-1}(m)}}{m^{\frac{n-1}{n}}} & m < m_{\mathrm{th}}, n > 0.5 \end{cases} \tag{A.45}$$

Appendix B

Post first shock formation

Consider the loading of an initially undeformed strain stiffening solid by the load (3.28) so that we have shocks. Let us assume that after a sufficiently long time from the first shock formation, a steady state pure shock propagates into the material, i.e there is a propagating velocity and strain discontinuity, with a velocity jump from 0 to V_0 and a strain jump from 0 to γ^- across the shock. The momentum balance equation (2.8) and the integral form of (2.13b), when applied to the case of a propagating pure shock, give us the jump conditions

$$\dot{s}[\![\gamma]\!] + [\![v]\!] = 0 \quad , \quad [\![\tau]\!] + \rho_0 \dot{s}[\![v]\!] = 0 \tag{B.1}$$

where, $\dot{s}$ is the shockspeed and $[\![f]\!] = f^+ - f^-$ denotes the jump in a field f across a shock, from its value f^+ ahead of the shock to f^- behind it. Eliminating $\dot{s}$ in (B.1) we obtain

$$[\![\tau]\!][\![\gamma]\!] = \rho_0 [\![v]\!]^2 \tag{B.2}$$

Using $\gamma^+ = \tau(\gamma^+) = v^+ = 0$, and $v^- = V_0$ in (B.2), and defining the auxiliary function $\phi(\gamma) = \tau(\gamma)\gamma$ we have

$$\phi(\gamma^-) = \rho_0 V_0^2 \tag{B.3}$$

Consider cases in which $t_{\text{shock}} > t_0$, that is the first shock does not form before the ramping is completed. Then the largest strain (in magnitude) realized before first shock formation, γ_1, would be the strain state at the trailing edge of the waveform where the velocity is equal to V_0, and is obtained from (using (3.2b), (2.15)^1, and definition of c in (2.11))

$$Q(\gamma_1) = \int_0^{\gamma_1} \sqrt{\frac{\tau'(\gamma)}{\rho_0}}\,\mathrm{d}\gamma = -V_0 \tag{B.4}$$

Squaring (B.4) and defining the non-dimensional auxiliary function $\chi(\gamma) = (\int_0^\gamma \sqrt{\tau'(\gamma)}\,\mathrm{d}\gamma)^2$ we obtain

$$\chi(\gamma_1) = \rho_0 V_0^2 \tag{B.5}$$

For a general strain stiffening solid the functions $\chi(\gamma)$ and $\phi(\gamma)$ are different, and hence, from (B.3) and (B.5) the strain state at the trailing edge of the evolving waveform, γ_1, is different from the strain state behind a steady state shock. As mentioned in Sec. 4.1, when applying the method of characteristics solution (2.17) behind the shock, $f(\beta)$ is not constant and the β characteristics come into play, meaning that there is also information traveling back to the loading surface from the growing shock. This might facilitate the change in strain state from γ_1 to γ^- for possible steady state shock propagation but this is subject for future research. See Ch. 4 in Hamilton et al. (1998) and the references therein for a discussion on reflection of waves by shocks in gas dynamics. There, it is demonstrated that for weak shock propagation the "reflected wave" is extremely small and can be neglected.

Bibliography

Aboudi, J., Benveniste, Y., 1973. One-dimensional finite amplitude wave propagation in a compressible elastic half-space. International Journal of Solids and Structures 9 (3), 363–378.

Aboudi, J., Benveniste, Y., 1974. Finite amplitude one-dimensional wave propagation in a thermoelastic half-space. International Journal of Solids and Structures 10 (3), 293–308.

Bland, D., 1965. On shock structure in a solid. IMA Journal of Applied Mathematics 1 (1), 56–75.

Budday, S., Sommer, G., Birkl, C., Langkammer, C., Haybaeck, J., Kohnert, J., Bauer, M., Paulsen, F., Steinmann, P., Kuhl, E., et al., 2017. Mechanical characterization of human brain tissue. Acta biomaterialia 48, 319–340.

Carroll, M., 1977a. Plane circular shearing of incompressible fluids and solids. The Quarterly Journal of Mechanics and Applied Mathematics 30 (2), 223–234.

Carroll, M., 1979. Reflection and transmission of circularly polarized elastic waves of finite amplitude. Journal of Applied Mechanics 46 (4), 867–872.

Carroll, M. M., Jun 1967. Some results on finite amplitude elastic waves. Acta Mechanica 3 (2), 167–181.

Carroll, M. M., Jan 1974. Oscillatory shearing of nonlinearly elastic solids. Zeitschrift für angewandte Mathematik und Physik ZAMP 25 (1), 83–88.

Carroll, M. M., Oct 1977b. Plane elastic standing waves of finite amplitude. Journal of Elasticity 7 (4), 411–424.

Catheline, S., Gennisson, J.-L., Tanter, M., Fink, M., 2003. Observation of shock transverse waves in elastic media. Physical review letters 91 (16), 164301.

Chu, B.-T., 1964. Finite amplitude waves in incompressible perfectly elastic materials. Journal of the Mechanics and Physics of Solids 12 (1), 45–57.

Chu, B.-T., 1967. Transverse shock waves in incompressible elastic solids. Journal of the Mechanics and Physics of Solids 15 (1), 1–14.

Collins, W., 1966. One-dimensional non-linear wave propagation in incompressible elastic materials. The Quarterly Journal of Mechanics and Applied Mathematics 19 (3), 259–328.

Collins, W., 1967. The propagation and interaction of one-dimensional non-linear waves in an incompressible isotropic elastic half-space. The Quarterly Journal of Mechanics and Applied Mathematics 20 (4), 429–452.

Davison, L., 1966. Propagation of plane waves of finite amplitude in elastic solids. Journal of the Mechanics and Physics of Solids 14 (5), 249–270.

Destrade, M., Murphy, J. G., Saccomandi, G., 2012. Simple shear is not so simple. International Journal of Non-Linear Mechanics 47 (2), 210–214.

Destrade, M., Pucci, E., Saccomandi, G., 2019. Generalization of the zabolotskaya equation to all incompressible isotropic elastic solids. Proceedings of the Royal Society A: Mathematical, Physical and Engineering Sciences 475 (2227), 20190061.

Destrade, M., Saccomandi, G., Jul 2005. Finite amplitude elastic waves propagating in compressible solids. Phys. Rev. E 72, 016620.

Espíndola, D., Lee, S., Pinton, G., 2017. Shear shock waves observed in the brain. Physical Review Applied 8 (4), 044024.

Fung, Y., 1993. Biomechanics: Mechanical Properties of Living Tissues. Biomechanics. Springer New York.

Gent, A., 1996. A new constitutive relation for rubber. Rubber chemistry and technology 69 (1), 59–61.

Hamilton, M. F., Blackstock, D. T., et al., 1998. Nonlinear acoustics. Vol. 237. Academic press San Diego.

Hamilton, M. F., Ilinskii, Y. A., Zabolotskaya, E. A., 2004. Separation of compressibility and shear deformation in the elastic energy density (l). The Journal of the Acoustical Society of America 116 (1), 41–44.

Horgan, C. O., 2015. The remarkable gent constitutive model for hyperelastic materials. International Journal of Non-Linear Mechanics 68, 9–16.

Horgan, C. O., Murphy, J. G., 2011. Simple shearing of soft biological tissues. In: Proceedings of the Royal Society of London A: Mathematical, Physical and Engineering Sciences. Vol. 467. The Royal Society, pp. 760–777.

Horgan, C. O., Murphy, J. G., 2012. A boundary-layer approach to stress analysis in the simple shearing of rubber blocks. Rubber Chemistry and Technology 85 (1), 108–119.

Lee-Bapty, I., Crighton, D., 1987. Nonlinear wave motion governed by the modified burgers equation. Philosophical Transactions of the Royal Society of London. Series A, Mathematical and Physical Sciences, 173–209.

Marchand, A., Duffy, J., 1988. An experimental study of the formation process of adiabatic shear bands in a structural steel. Journal of the Mechanics and Physics of Solids 36 (3), 251–283.

Mercier, S., Molinari, A., 1998. Steady-state shear band propagation under dynamic conditions. Journal of the Mechanics and Physics of Solids 46 (8), 1463–1495.

Mihai, L. A., Budday, S., Holzapfel, G. A., Kuhl, E., Goriely, A., 2017. A family of hyperelastic models for human brain tissue. Journal of the Mechanics and Physics of Solids 106, 60–79.

Mihai, L. A., Chin, L., Janmey, P. A., Goriely, A., 2015. A comparison of hyperelastic constitutive models applicable to brain and fat tissues. Journal of The Royal Society Interface 12 (110), 20150486.

Mooney, M., 1940. A theory of large elastic deformation. Journal of applied physics 11 (9), 582–592.

Ogden, R. W., 1972. Large deformation isotropic elasticity–on the correlation of theory and experiment for incompressible rubberlike solids. Proceedings of the Royal Society of London. A. Mathematical and Physical Sciences 326 (1567), 565–584.

Pogoda, K., Chin, L., Georges, P. C., Byfield, F. J., Bucki, R., Kim, R., Weaver, M., Wells, R. G., Marcinkiewicz, C., Janmey, P. A., 2014. Compression stiffening of brain and its effect on mechanosensing by glioma cells. New journal of physics 16 (7), 075002.

Rivlin, R., 1948. Large elastic deformations of isotropic materials iv. further developments of the general theory. Phil. Trans. R. Soc. Lond. A 241 (835), 379–397.

Storm, C., Pastore, J. J., MacKintosh, F. C., Lubensky, T. C., Janmey, P. A., 2005. Nonlinear elasticity in biological gels. Nature 435 (7039), 191.

Wochner, M. S., Hamilton, M. F., Ilinskii, Y. A., Zabolotskaya, E. A., 2008. Cubic nonlinearity in shear wave beams with different polarizations. The Journal of the Acoustical Society of America 123 (5), 2488–2495.

Zabolotskaya, E., 1986. Sound beams in a nonlinear isotropic solid. SOVIET PHYSICS ACOUSTICS-USSR 32 (4), 296–299.

Zabolotskaya, E. A., Hamilton, M. F., Ilinskii, Y. A., Meegan, G. D., 2004. Modeling of nonlinear shear waves in soft solids. The Journal of the Acoustical Society of America 116 (5), 2807–2813.

Ziv, R., Shmuel, G., 2019. Smooth waves and shocks of finite amplitude in soft materials. Mechanics of Materials 135, 67 – 76.